Flavonols and dihydroflavonols inhibit the main protease activity of SARS-CoV-2 and the replication of human coronavirus 229E

Yue Zhu[1], Frank Scholle[2], Samantha C. Kisthardt[2] De-Yu Xie[1]*

1, Department of Plant and Microbial Biology, North Carolina State University, Raleigh, NC, USA.

2, Department of Biology, North Carolina State University, Raleigh, NC, USA.

* Corresponding author, dxie@ncsu.edu

Abstract

Since December 2019, the deadly novel severe acute respiratory syndrome coronavirus 2 (SARS-CoV-2) has caused the current COVID-19 pandemic. To date, vaccines are available in the developed countries to prevent the infection of this virus, however, medicines are necessary to help control COVID-19. Human coronavirus 229E (HCoV-229E) causes the common cold. The main protease (M^{pro}) is an essential enzyme required for the multiplication of these two viruses in the host cells, and thus is an appropriate candidate to screen potential medicinal compounds. Flavonols and dihydroflavonols are two groups of plant flavonoids. In this study, we report docking simulation with two M^{pro} enzymes and five flavonols and three dihydroflavonols, *in vitro* inhibition of the SARS-CoV-2 M^{pro}, and *in vitro* inhibition of the HCoV 229E replication. The docking simulation results predicted that (+)-dihydrokaempferol, (+)-dihydroquercetin, (+)-dihydromyricetin, kaempferol, quercetin, myricentin, isoquercetin, and rutin could bind to at least two subsites (S1, S1', S2, and S4) in the binding pocket and inhibit the activity of SARS-CoV-2 M^{pro}. Their affinity scores ranged from -8.8 to -7.4. Likewise, these compounds were predicted to bind and inhibit the HCoV-229E M^{pro} activity with affinity scores ranging from -7.1 to -7.8. *In vitro* inhibition assays showed that seven available compounds effectively inhibited the SARS-CoV-2 M^{pro} activity and their IC50 values ranged from 0.125 to 12.9 μM. Five compounds inhibited the replication of HCoV-229E in Huh-7 cells. These findings indicate that these antioxidative flavonols and dihydroflavonols are promising candidates for curbing the two viruses.

Keywords: (+)-dihydrokaempferol, (+)-dihydroquercetin, (+)-dihydromyricetin, kaempferol, quercetin, myricentin, isoquercetin, rutin, flavan-3-ols

1. Introduction

SARS-CoV-2 is the abbreviation of the novel severe acute respiratory syndrome coronavirus 2. This virus was firstly reported to cause a severe pneumonia in December of 2019 in Wuhan, China [1-3]. On February 11, 2020, the World Health Organization (WHO) designated this pneumonia as coronavirus disease 2019 (COVID-19). COVID-19 the rapidly spread different countries. On March 11, 2020, WHO announced the COVID-19 pandemic [4,5]. This pandemic has rapidly spread across all over the world. By June 21, 2021, based on the COVID-19 Dashboard by Center for Systems Science and Engineering at Johns Hopkins Coronavirus Resource Center, 117,553,726 infected cases and 3,867,641 deaths have been reported from more than 200 countries or regions. No strategy to stop the spread of this virus was available until January 2021, when several vaccines started to be approved for vaccination in several countries [6-11]. On one hand, since the start of vaccination, the number of infections has started to decrease. On the other hand, due to the insufficient vaccine quantities and vaccine hesitancy even where available, in the first week of February, 2021, the daily infection cases and deaths were still more than 400,000 and 11,000, respectively. By Feb. 9, the case numbers still increased by more than 300,000 daily. Meanwhile, the use of vaccines has also indicated that developing effective medicines is necessary to stop COVID-19. A recent study showed that mutations in the spike protein of SARS-CoV-2 might cause the escape of new variants from antibody [12]. The variant B.1.351 found in South Africa was reported to be able to escape vaccines developed by AstraZeneca, Johnson & Johnson (J&J), and Novavax [13]. Merck & Co has stopped their race for vaccines due to the

lack of effectiveness of their products, instead, they continue to focus on antiviral drug development [14]. Unfortunately, to date, effective medicines are still under screening. Although chloroquine and hydroxychloroquine were reported to be potentially effective in helping to improve COVID-19 [15], the use of these two anti-malarial medicines has been arguable in USA because of potential risk concerns [16]. Other potential candidate medicines are the combination of α-interferon and anti-HIV drugs lopinavir/ritonavir [17], and remdesivir [15,18]. Given that the efficacy of all these medicines being repurposed has not been conclusive, further studies are necessary to apply them for treating COVID-19.

SARS-CoV-2 is a single stranded RNA virus. Its genomic RNA contains around 30,000 nucleotides and forms a positive sense strand with a 5′ methylated cap and a 3′ polyadenylated tail that encodes at least six open reading frames (ORF) [19,20]. This feature allows it to be able to use the ribosomes of the host cells to translate proteins. The longest ORF (ORF1a/b) translates two polyproteins, which are cleaved by one main protease (M^{pro}, a 3C-like protease, $3CL^{pro}$) and another papain-like protease (PL2pro) into 16 nonstructural proteins (NSPs), which include RNA-dependent RNA polymerase (RdRp, nsp12), RNA helicase (nsp13), and exoribonuclease (nsp14). The NSPs subsequently produce structural and accessory proteins. The structural proteins include an envelope protein, membrane protein, spike (S) protein, and nucleocapsid protein (Fig.1) [21,22]. The S protein is a type of glycoprotein and plays an essential role in the attachment and the infection of the host cells [23]. It binds to the human angiotensin converting enzyme 2 to help the virus enter the human cells [24,25]. Since May 2020, the mutations of amino acids of the S protein has created a

large number of variants, of which the emergence of alpha, beta, gamma, and delta variants has shown more pathogenic and transmissible, thus caused potential challenges to use vaccines to completely control the pandemic [26-30].

Human coronavirus 229E (HCoV-229E) is a pathogenic virus in the genus *Alphacoronavirus* [31]. It is one of the causative viral agents of the common cold [32,33]. Its genome consists of a positive sense and single-stranded RNA with 27,317 nucleotides (nt). Its genome size commonly varies in different clinical isolates. For example, HCoV-229E strains 0349 and J0304 were two clinical isolates causing the common cold [34]. The entire genome of these two clinical isolates were reported to be about 27, 240 nt, which included 38.07 % GC content is in 0349 and 38.13 % GC content in J0304. In general, the genome of HCoV-229E is characterized with a gene order of 5'-replicase ORF1a/b, spike (S), envelope (E), membrane (M), nucleocapsid (N)-3' [35], Like SARS-CoV-2, the spike protein is the determinant of infections to host cells [36]. The ORF1a/b of HCoV-229E encodes 16 non-structural proteins (NSPs). The *NSP5* encodes the M^{pro} that is required for the replication in the host cells [34]. Given that HCoV-229E is allowed to be studied in BSL2 laboratories, this pathogenic virus is an appropriate model to screen therapeutics for the treatment of both common cold and COVID-19.

Given that the SARS-CoV-2 M^{pro} not only plays a vital role in the cleavage of polyproteins, and there is no human homolog, it is an ideal target for anti-SARS-CoV-2 drug screens and development [37,38]. It belongs to the family of cysteine proteases and has a Cys-His catalytic

dyad, which is an appropriate site to design and screen antiviral drugs [39]. Its high-resolution crystal structure was elucidated in April 2020 [40]. Based on the crystal structure, screening the existing antiviral medicines or designed chemicals revealed that cinanserin, ebselen, GC376, 11a, and 11b showed inhibitory effects on the M^{pro} activity [39-43]. A common feature is that these molecules deliver their carbonyl group (aldehyde group or ketone group) to the thiol of the 145 cysteine residue to form a covalent linkage, thus inhibit the M^{pro} activity. The potential application of these molecules is still under studies to evaluate their effectiveness and side effects. In addition, we recently found that flavan-3-ol gallates, such as (-)-epigallotechin-3-gallate, (-)-catechin-3-gallate, and (-)-epicatechin-3-gallate, and dimeric procyanidins promisingly inhibited the M^{pro} activity [44]. Docking simulation indicated that their inhibitory activity likely resulted from the formation of hydrogen bonds between these compounds and several amino acids in the binding domain of M^{pro}.

Flavonols and dihydroflavonols (Fig. 2) are two main groups of plant flavonoids [45,46]. Quercetin, kaempferol, and myricetin are three flavonol molecules widely existing in plants. Likewise, dihydroquercetin, dihydrokaempferol, and dihydromyricetin are three dihydroflavonol molecules in plants [47,48]. In general, flavonols and dihydroflavonols are strong antioxidants with multiple benefits to human health [49-58]. Furthermore, studies have reported that quercetin and its derivatives have antiviral activity [59-61]. Based on these previous findings, we hypothesized that flavonols and dihydroflavonols might inhibit the M^{pro} activity of SARS-CoV-2 and HCoV-229E. In this study, to test this hypothesis, we performed docking simulation for three dihydroflavonols, three flavonols, and two glycosylated

quercetins. Then, we tested these compound's inhibition against the recombinant M^{pro} activity of SARS-CoV-2 *in vitro*. More importantly, five available compounds were evaluated to determine their inhibitive activity against the replication of HCoV-229E in Huh-7 cells. The resulting data showed eight compounds effectively inhibited the M^{pro} activity of SARS-CoV-2 and five tested compounds inhibited the replication of HCoV-229E in Huh-7 cells.

2. Materials and methods

2.1 Dihydroflavonols, flavonols, cell line, and coronavirus

Flavonols used in this study included kaempferol, quercetin, myricetin, quercetin-3-O-glycoside, and rutin. Dihydroflavonols used were (+)-taxifolin (dihydroquercetin, DHQ), (+)-dihydrokaempferol (DHK), and (+)-dihydromyricetin (DHM). Two flavan-3-ols, (-)-epicatechin and (+)-catechin, were used as compound controls. The ebselen was used as a positive control. These compounds were purchased from Sigma-Aldrich (https://www.sigmaaldrich.com/)

Huh-7 cells, a human hepatocellular carcinoma cell line, are an appropriate to study the replication of different viruses [62-66]. This cell line was used for infection and propagation of virus and for testing antiviral activity of compounds. Human coronavirus 229E (HCoV-229E) is a positive sense and single-stranded RNA virus that infects the human respiratory system

[67-71]. HCoV-229E was propagated on Huh-7 cells and tittered by TCID50 assay.

2.2 Docking simulation of the SARS-CoV-2 M^{pro}

We recently reported the docking simulation of flavan-3-ols, such as epicatechin and catechin (Fig. 2) [44]. Herein, we used the same steps for docking simulation of flavonols and dihydroflavonols in this experiment. In brief, three main steps were completed, protein preparation, ligand preparation, and protein-ligand docking. The first step was protein preparation. The SARS-CoV-2 M^{pro} was used as a receptor to test ligands. Its ID is PDB ID: 6LU7 at Protein Data bank (https://www.rcsb.org/), from which its 3D structure was downloaded to a desktop computer and then was prepared as a receptor of ligand via the Dock Prep tool of UCSF-Chimera (https://www.cgl.ucsf.edu/chimera/). Because M^{pro} contains the inhibitor peptide N3, we removed N3 prior to docking simulation. Hydrogens and charges were added and optimized to allow determining the histidine protonation state. The second step was ligand preparation. The 3D structures of compounds (Fig. 2) were obtained from PubChem (https://pubchem.ncbi.nlm.nih.gov/) and then used as ligands. All structures were minimized by using the minimize structure tool of UCSF-Chimera. Hydrogens and charges were added to the ligands, which were then saved as mol2 format for the protein-ligand docking simulation. The third step was protein-ligand docking. The modeling of protein-ligand docking was performed via the publically available AutoDock Vina (http://vina.scripps.edu/) software. The protein and ligand files were loaded to the AutoDock Vina through the UCSF-Chimera surface binding analysis tools. A working box

was created to contain the whole receptor. The box center was set at x =-27, y = 13, and z = 58. The box size was set as x = 50, y =55, and z = 50, which framed the entire receptor to allow free position changes and ligand binding to the receptor at any potential positions.

2.3 Docking simulation of the HCoV-229E M^{pro}

HCoV-229E needs a M^{pro} (3C-like protease) for its replication in the host cells [72-74]. The M^{pro} is also a target for screening anti-HCoV-229E medicines [75-77]. The sequence of the HCoV-229E M^{pro} was obtained from the GenBank and then used for an alignment and docking simulation. The steps of simulation were the same as described above.

2.4 Inhibition assay of the SARS-CoV-2 M^{pro} activity

(+)-DHQ, (+)-DHK, (+)-DHM, quercetin, kaempferol, myricetin, quercetin-3-O-glycoside, rutin, (-)-epicatechin, and (+)-catechin were dissolved in DMSO to prepare a 1.0 M solution. A SARS-CoV-2 Assay Kit (BPS bioscience, https://bpsbioscience.com/) was used to test the inhibitory activity of these compounds. The steps of *in vitro* assay followed the manufacturer's protocol as performed in our recent report [44]. In brief, each reaction was carried out in a 25 µl volume in 384-well plates. Each reaction solution contains 150 ng recombinant M^{pro} (6 ng/µl), 1 mM DDT, 50 µM fluorogenic substrate, and one compound (0, 0.02, 0.05, 0.1, 0.5, 1, 5, 10, 50, 100, 150, and 200 µM) in pH 8.0 mM Tris-HCl and 5 µM EDTA buffer. GC376 (50 µM) was used as a positive control, while (-)-epicatechin and

(+)-catechin were used as two negative controls. The reaction mixtures were incubated for 2 hrs at room temperature. The fluorescence intensity of each reaction was measured and recorded on a microtiter plate-reading fluorimeter (BioTek's Synergy H4 Plate Reader for detect fluorescent and luminescent signals). The excitation wavelength was 360 nm and the detection emission wavelength was 460 nm. Each concentration of every compound was tested five times. A mean value was calculated with five individual replicates. Plots were built with the percentiles of catalysis versus log [μM] values of concentrations to show the effect of each compound on the M^{pro} activity. Statistical evolution is described below.

2.5 Inhibition assay of Human coronavirus 229E

Huh-7 cells were grown in Dulbecco's Modified Eagle Medium (DMEM) supplemented with 10% fetal bovine serum (10% FBS) and 1% antibiotics. HCoV-229E was propagated on Huh-7 cells. Virus containing supernatants were harvested 72h post infection and stored at -80°C. The virus titer was determined by the Median Tissue Culture Infectious Dose 50 (TCID50) assay in Huh-7 cells.

Then, we performed virus inhibition assays. Huh-7 cells were seeded in 96 well plates at a density of 25,000 cells/well and incubated overnight. HCoV 229-E was diluted in MEM with 1% FBS, 1% HEPES buffer, and 1% antibiotic solution (MEM 1+1+1). The cells were inoculated with HCoV-229E at an MOI of 1 in a total volume of 50 μl. The infected plates were incubated at 35°C with 5% CO2 for one hour. Phytochemicals dissolved in DMSO were

added in cell culture medium to the following concentrations: 0 µM, 2.5 µM, 5 µM, 10 µM, 20 µM, and 50 µM.

After one hour, virus and medium were removed from the infected cells and washed once with 200ul of PBS. 100 µl of each compound master mix was added to triplicate wells for each concentration. Virus was allowed to grow in the presence of each compound at 35 °C and 5% CO2 for 24 hours. Supernatants were harvested and virus titers on Huh-7 cells were determined by TCID50 assay [78]. Plates were incubated at 37°C and 5% CO2 for 96 hours, inspected visually for cytopathic effect (CPE) and TCID50/mL was calculated using the Spearman-Kaerber method [79,80]. A mean value was calculated using three replicates. Plots were built with TCID50/mL versus concentrations to show the effect of each compound on the replication of virus in Huh-7 cells. The minimum level of detection in this assay was 632 TCID50/ml.

2.6 Statistical evaluation

One-way analysis of variance (ANOVA) was performed to evaluate the statistical significance. The P-value less than 0.05 means significant differences.

3. Results

3.1 Ligand-receptor docking of flavonols and dihydroflavonols to the M^{pro} of

SARS-CoV-2

Docking simulation was completed with the UCSF-Chimera and AutoDock Vina software to evaluate the binding abilities of flavonols and dihydroflavonols to the SARS-CoV-2 M^{pro}. The M^{pro} structure is featured with a substrate-binding pocket (Fig.3). When the 3D structure of the protein was downloaded from the public database, the peptide inhibitor N3 was shown to bind to this pocket. During protein preparation, N3 was removed for docking. The simulation results showed that (+)-DHQ, (+)-DHK, (+)-DHM, quercetin, kaempferol, myricetin, quercetin-3-O-glycoside, rutin, (-)-epicatechin, (+)-catechin, and ebselen bound to the binding pocket (Fig. 3). The resulting affinity scores for (+)-DHQ, (+)-DHK, (+)-DHM, quercetin, kaempferol, myricetin, quercetin-3-O-glycoside, and rutin ranged from -8.8 to -7.4, lower and better than the score of ebselen (-6.6) (Table 1). The scores among the aglycones of (-)-epicatechin, (+)-catechin, three dihydroflavonols, and three flavonol aglycones were close, either -7.4 or -7.5. These data suggested that dihydroflavonols, flavonols, and glycosylated flavonols could potentially inhibit the M^{pro} activity.

3.2 Docking features at the binding pocket of the SARS-CoV-2 M^{pro}

As we reported recently [44], the M^{pro} substrate-binding pocket includes four subsites, S1', S1, S2, and S4. Cys145 is a critical residue located at the space among subsites S1, S1', and S2 (Fig.4a) [39,40]. Several studies have reported that the thoil of the Cys145 residue is crucial for the catalytic activity of M^{pro} and if a compound binds to this residue, it can inhibit the

M^{pro} activity [21,39,42]. When ebselen was used as our positive compound for simulation, as we reported recently [44], it bound to this residue featured by three rings facing to the S1 and S1' subsites (Fig. 4 b). The docking simulation results showed that three dihydroflavonols, three flavonols aglycones, and two glycosylated flavonols bound to 2 to 4 subsites via the Cys145 residue. In three dihydroflavonols tested, (+)-DHK and (+)-DHQ showed a difference in their occupation in the binding site. The A and B rings of (+)-DHK and (+)-DHQ dwelled in the S1' and S2 subsites and their heterocycle C ring resided in the space between the S1 and S2 subsites (Fig. 4 c-d). The A and B rings of DHM occupied the S1 and S4 subsites and the heterocycle C ring resided in the space between the S1 and S2 subsites (Fig. 4 e). In three flavonol aglycones tested, the occupation of kaempferol was different from that of quercetin and myricetin. The A-ring, B-ring, and heterocycle C-ring of kaempferol resided in the S1', S2, and the space between S1 and S2, respectively (Fig. 4f). The A-ring, B-ring, and the heterocycle C-ring of quercetin and myricetin dwelled in the S1, S4, and the space between S1 and S2 (Fig. 4 g-h). In comparison, the residing positions of isoquercitrin and rutin were more complicated. The A-ring, B-ring, heterocycle C-ring, and 3-glucose of isoquercitrin occupied the S2, S1', the space between S1 and S2, and S1 (Fig. 2 i). The A-ring, B-ring, heterocycle C-ring, 6-β-glucopyranose, and 1-L-α-rhamnopyranose of rutin occupied S4, S1', the space between S1/S2, S1, and S4 (Fig. 4 j). These occupations in the binding sites suggested that these compounds might have an inhibitive activity against M^{pro}.

3.3 Ligand-receptor docking of flavonols and dihydroflavonols to the M^{pro} of HCoV-229E

The M^{pro} of HCoV-229E was also used for docking simulation. A sequence alignment revealed that the identity of between the two M^{pro} homologs of HCoV-229E and SARS-CoV-2 was 42.81% (Figure 5 a). The binding domains were highly conserved. Furthermore, a 3D modeling revealed that the conformation and binding pocket of the HCoV-229E M^{pro} were similar to those of SARS-CoV-2 M^{pro} (Fig. 5 b and c). The simulation results were the same as those of the M^{pro} of SARS-CoV-2 described above. (+)-DHQ, (+)-DHK, (+)-DHM, quercetin, kaempferol, myricetin, quercetin-3-O-glycoside, rutin, (-)-epicatechin, (+)-catechin, and ebselen could bind to the binding pocket of the HCoV-229E M^{pro} (Fig. 6). The affinity scores of these compounds ranged from -7.8 to - 7.1 (Table 1). The scores of rutin and isoquercitrin (two glycosides) binding to the HCoV-229E M^{pro} were -7.8 and -7.5, higher than -8,8 and -8.7, the scores of the two compounds binding to the SARS-CoV-2 M^{pro} (Table 1). This result indicates that compared with the affinity score of quercetin, these two types of glycosylation reduce the affinity scores binding to the SARS-CoV-2 M^{pro}, but do not affect the affinity scores binding to the HCoV-229E M^{pro}.

3.4 *In vitro* inhibitory effects of five flavonols and two dihydroflavonols on the SARS-CoV-2 M^{pro} activity

(+)-DHQ, (+)-DHM, quercetin, kaempferol, myricetin, isoquercetin (quercetin-3-O-glycoside), and rutin were used to test their inhibitory effects on the M^{pro} activity. In addition, based on our recent report [44], (-)-epicatechin and (+)-catechin were

used as negative controls. The resulting data showed that (+)-DHQ, (+)-DHK, (+)-DHM, quercetin, kaempferol, myricetin, isoquercetin (quercetin-3-O-glycoside), and rutin inhibited the SARS-CoV-2 M^{pro} activity. The half maximum inhibitory concentrations (IC50) were 0.125-12.94 μM (Fig. 7). Among the tested seven compounds, rutin had the lowest IC5 value with the most effectiveness to inhibit the M^{pro} activity (Fig. 7 g), while (+)-DHQ had the highest IC50 value with the lowest inhibitive activity (Fig. 7 d). One hundred μM was used to further compare the inhibitive effects of these compounds on the M^{pro} activity in a given time. The resulting data showed the most effectiveness of rutin (Fig. 7 h). In addition, as we reported previously, (+)-catechin and (-)-epicatechin did not show an inhibitory effect on the M^{pro} activity in the range of concentrations from 0-200 μM. For example, the two compounds did not inhibit the catalytic activity of the M^{pro} at 100 μM (Fig. 7 h).

3.5 Inhibitory effects of five compounds on the replication of HCoV-229E in Huh-7 cells

Quercetin, isoquercetin, taxifolin, were tested their inhibitory effects on the replication of HCoV-229E in Huh-7 cells. In addition, epigallocatechin gallate (EGCG), and epicatechin two examples of flavan-3-ols, were tested. The reason was that we recently reported that EGCG effectively inhibited the SARS-CoV-2 M^{pro} activity, while epicatechin could not [44], however whether they could inhibit coronavirus replication in the host cells was untested. It was essential to test them. The resulting data indicated that all five compounds showed an inhibition against the replication of HCoV-229E in Huh-7 cells (Figure 8). Based on TCID50/ml values, taxifolin started to show its inhibition at 2.5 μM and its inhibitory activity

increased as its concentration was increased. Quercetin started to have inhibition at 5 μM. As its concentrations were increased, its inhibitive activities were more effective. At a concentration tested higher 10 μM, quercetin could strongly inhibit the replication of the virus. Its EC50 value was estimated to be 4.88 μM (Figure 8 b). Isoquercitrin strongly inhibited the replication starting with 2.5 μM. EGCG started to show its inhibition against the replication of the virus at 2.5 μM and its inhibition became stronger as its concentrations were increased. It was interesting that epicatechin could strongly inhibit the replication starting at 20 μM.

4. Discussion

The development of medicines is necessary to complement the use of vaccines to control COVID-19. The SARS-CoV-2 M^{pro} is one of the targets to screen, repurpose, or develop drugs to treat or prevent SARS-CoV-2 [21,22,39]. One strategy is to inhibit the M^{pro} activity via delivering a compound to the Cys145 residue at the space across the region of S1' and S1 subsites [39]. Ebselen is a small molecule candidate that has been found to inhibit the M^{pro} activity with an IC_{50} 0.46 μM [40]. Its structure featured with three rings was revealed to be an effective vessel to deliver its carbonyl group to the CYS145 residue (Fig. 4 b). We recently reported another strategy. We have found that epicatechin gallate, epigallocatechin gallate, gallocatechin gallate, catechin gallate, and procyanidin B2 could effectively inhibited the activity of M^{pro} via the formation of hydrogen bonds with different amino acids in the binding pocket [44]. Our findings indicated that the formation of peptide bonds was effective to screen

more flavonoids to intervene COVID-19. Quercetin and other flavonols are common nutraceuticals with antiviral activities, such as influenza virus, hepatitis B virus, Zika virus, and Ebola viruses [59,81-83]. In this study, we took advantage of our recent strategy to perform this docking simulation of flavonols and dihydroflavonols. These two groups of compounds (Figs. 2 and 4) have C4 keto and 3-OH structures in the heterocycle C-ring. Like flavan-3-ol gallates, the structures of these two groups might have a potential to reside in the space S1 and S2 subsites. In the present study, our ligand-docking simulation showed that these two groups of compounds could bind to the substrate-binding pocket of M^{pro} and occupied their heterocyclic C ring in the crossing region between S1 and S2. Furthermore, the docking results predicted the A-ring and B-ring of two, three, two, and one compounds could bind to S1' and S2, S1 and S4, S2 and S1', and S4 and S1', respectively (Fig. 4). The docking results further showed that a glycosylation of quercetin increased the dwelling capacity in the binding site. Rutin was predicted to occupy all four subsites (Fig. 4 j). The increase of binding subsites was also reflected by the affinity scores of M^{pro}-ligands. Rutin and isoquercitrin had the lowest and second lowest score values (Table 1). These data indicated that not only might these compounds have an inhibitive activity but also a lower and better affinity score might indicate a strong inhibition against the M^{pro} activity. Further *in vitro* assays substantiated the prediction of docking simulation. Seven available compounds inhibited the activity of M^{pro} with IC5 values from 0.125 to 12.9 μM. These data imply that these compounds might be potential therapeutics.

Given that SARS-CoV-2 can be only handled in the BSL-3 laboratories, we cannot access

this deadly virus to test the effects of these compounds on its replication in host cells. Instead, we selected the less pathogenic HCoV-229E to test the inhibitory activity of these compounds. We hypothesized that inhibitory compounds screened against this virus might be appropriate for the potential therapy of COVID-19. The reason is that like SARS-CoV-2, the replication of HCoV-229E also depends on its M^{pro} activity in human cells and the active site is highly conserved between HCoV229E and SARS-CoV-2. Accordingly, the resulting data might help design medicines for the therapy of both COVID-19 and HCoV-229E respiratory diseases. An amino sequence alignment revealed that the identity of HCoV-229E and SARS-CoV-2 M^{pro} homologs was approximately 48%. The binding domain of substrates between the two homologs was conserved. Docking simulation and the resulting affinity scores further indicated that these compounds could reside in the binding pocket to potentially inhibit the activity of the M^{pro} of HCoV-229E (Fig. 4 and Table 1). Based on these data, we could test five compounds with HCoV-229E. In tested concentrations, taxifolin and isoquercitrin starting from 2.5 μM showed a significant inhibition of HCoV-229E replication in Huh-7 cells. Quercetin could slightly reduce the replication of HCoV-229E at 2.5 μM and significantly inhibited the replication of this virus at higher concentrations (Fig. 8 a). These positive results not only supported the docking simulation results that these compounds bound to the M^{pro} of HCoV-229E (Table 1), but also substantiated the results of *in vitro* assays that these compounds effectively inhibited the SARS-CoV-2 M^{pro} activity (Fig. 7). We previously demonstrated that EGCG could effectively inhibit the activity of the SARS-CoV-2 M^{pro} [44]. Herein, we used it as a positive control. The resulting data showed that EGCG starting with 2.5 μM could significantly inhibit the replication of HCoV-229E in Huh-7 cells.

This positive control result further supported that taxifolin, isoquercitrin and quercetin inhibited the replication of HCoV-29E via the reduction of the M^{pro} activity. In addition, we tested epicatechin, which was not shown to have an inhibitive activity against the SARS-CoV-2 M^{pro} in our vitro assays. It was interesting that epicatechin starting with 20 μM tested could inhibit the replication of HCoV-229E (Fig. 8 a), which was supported by the results of the docking simulation and its affinity score (Fig. 6 and Table 1). Accordingly, this datum indicates the difference between HCoV-229E and SARS-CoV-2. Taken together, these data indicate that HCoV-229E is appropriate substitute to screen inhibitors of SARS-CoV-2 by targeting the M^{pro} of these two viruses.

Quercetin, isoquercitrin and rutin are three common supplements, given that their nutritional values benefit human health [84-89]. Our data suggest that quercetin, isoquercitrin, and rutin might be helpful to intervene COVID-19. These compounds are plant natural flavonoids that their bio-availability, metabolism, and toxicity have been studied extensively [46]. In general, these compounds are safe nutrients sold as supplements or in food products such as onion and common dinner table fruits [90-95]. More importantly, quercetin can be absorbed into the human body from the intestines. A large number of human health studies have reported the presence of quercetin and its derivatives in the blood plasma and their nutritional benefits after consumption [96-99]. For example, the quercetin concentration in plasma was reported to reach 5.0±1.0 μM after the intake of 150 mg in one hour [100,101]. In addition, these compounds are potent antioxidants [102,103]. The intake of quercetin can inhibit the oxidation of LDL and prevent the cardiovascular diseases [101,104] [105]. Moreover, quercetin and its

derivatives have strong anti-inflammation activity [106-110]. All of these functions can benefit people's health.

Figure legends

Figure 1 A diagram showing the function of the SARS-CoV-2 main protease in the virus replication in the host cells. Once the virus enters into the host cells. Its positive sense and single stranded RNA uses the ribosomes to translate open reading frames 1a and 1b to polyproteins (PP), in which the main protease and papain-like protease cleaves PPs to non-structural proteins (NSPs). Three NSPs, RNA dependent RNA polymerase (RdRp), RNA helicase, and exoribonuclease, are involved in the transcription of the positive RNA to negative sense and single stranded RNA, which is further transcribed to positive sense and single stranded RNA. Finally, structural proteins and a positive single stranded RNA assembly together to form a virus progeny.

Figure 2 Structures of ebselen and 10 flavonoids. Two flavan-3-ols: (-)-epicatechin and (+)-catechin; three dihydroflavonol aglycones: (+)-dihydroquercetin, (+)-dihydrokaempferol, and (+)-dihydroquercetin; three flavonols aglycones, kaempferol, quercetin, and myricetin; two glycosylated flavonols: quercetin-3-O-glycoside (isoquercitrin), and rutin.

Figure 3 Ligand-receptor docking modeling showing the binding of eleven compounds to the substrate pocket of the SARS-CoV-2 main protease (M^{pro}). The first image shows the 3D

surface view of the SARS-CoV-2 M^{pro}, on which the red rectangular frame indicates the substrate-binding pocket. Eleven flavonoids and ebselen bind to this pocket. Two flavan-3-ols: (+)-catechin (CA) and (-)-epicatechin (EC); three dihydroflavonol aglycones: (+)-dihydroquercetin (DHQ), (+)-dihydrokaempferol (DHK), and (+)-dihydroquercetin (DHM); three flavonols aglycones, kaempferol, quercetin, and myricetin; two glycosylated flavonols: quercetin-3-O-glycoside (isoquercitrin), and rutin.

Figure 4 Orientation features of compounds binding to subsites. a, a surface image shows the four subsites in the binding pocket. b-j, images show the binding positions of nine compounds. Two flavan-3-ols: (+)-catechin (CA) and (-)-epicatechin (EC); three dihydroflavonol aglycones: (+)-dihydroquercetin (DHQ), (+)-dihydrokaempferol (DHK), and (+)-dihydroquercetin (DHM); three flavonols aglycones, kaempferol, quercetin, and myricetin; two glycosylated flavonols: quercetin-3-O-glycoside (isoquercitrin), and rutin.

Figure 5 Amino acid sequence alignment of the SARS-CoV-2's and HCoV-229E's M^{pro} homologs and comparison of their three dimensional (3D) models. a, amino sequence alignment, in which three rectangle frames highlight three conserved domains forming the substrate binding pocket; b, a comparison of the 3D models of the SARS-CoV-2's (bronze color) and HCoV-229E's (blue color) M^{pro} homologs; c, yellowish, orange, and reddish colors showing the binding pocket formed from three conserved binding domains highlighted with three rectangle frames in a, in which the reddish and yellowish spaces include Cys-His catalytic dyad.

Figure 6 Ligand-receptor docking modeling showing the binding of eleven compounds to the substrate pocket of the HCoV-229E main protease. The first image shows the 3D surface view of the HCoV-229E M^{pro}, on which the red rectangular frame indicates the substrate-binding pocket. Eleven flavonoids and ebselen bind to this pocket. Two flavan-3-ols: (+)-catechin (CA) and (-)-epicatechin (EC); three dihydroflavonol aglycones: (+)-dihydroquercetin (DHQ), (+)-dihydrokaempferol (DHK), and (+)-dihydroquercetin (DHM); three flavonols aglycones, kaempferol, quercetin, and myricetin; two glycosylated flavonols: quercetin-3-O-glycoside (isoquercitrin), and rutin.

Figure 7 Inhibitory effects of nine compounds on the M^{pro} activity of SARS-CoV-2. a-g, seven plots show the inhibitory curves of seven compounds against the M^{pro} activity. All dots in each plot are an average value calculated from five replicates. IC50 value for each compound is inserted in each plot. “95% Cl” means 95% confidence internal. “(value 1, value 2)” means values in the range with 95% Cl. h, a comparison shows the inhibitory effects of 11 compounds at 100 μM on the M^{pro} activity. GC376 is an inhibitor used as positive control. (+)-catechin, (-)-epicatechin, and water are used as negative controls. Two flavan-3-ols: (+)-catechin (Ca) and (-)-epicatechin (Ep); three dihydroflavonol aglycones: (+)-dihydroquercetin (DHQ), (+)-dihydrokaempferol (DHK), and (+)-dihydroquercetin (DHM); three flavonols aglycones, kaempferol (Ka), quercetin (Qu), and myricetin (My); two glycosylated flavonols: quercetin-3-O-glycoside (isoquercitrin, Iso), and rutin.

Figure 8 Inhibition of five compounds on the replication of HCoV-229E in Huh-7 cells. a, plots were built with TCID50/mL versus concentrations of each compound. b, this plot was built with the inhibition rate (%) versus log [μM] values to estimate the EC50 of quercetin. “95% Cl” means 95% confidence internal. “(value 1, value 2)” means values in the range with 95% Cl. Bars labeled with “*” means were significant difference compared with control without adding compounds (P-value less than 0.05).

Table 1 Affinity scores of 11 compounds binding to the main proteases of SARS-CoV-2 and HuCoV-229E

Compounds	Affinity score (SARS-CoV-2)	Affinity score (229E)	Molecular weight (Da)
Rutin	-8.8	-7.8	610.5
Isoquercitrin	-8.7	-7.5	464.1
Kaempferol	-7.7	-7.6	286.2
DHK	-7.6	-7.6	288.2
DHM	-7.5	-7.6	320.2
Myricetin	-7.4	-7.1	318.2
Quercetin	-7.4	-7.7	302.2
(+)-Taxifolin	-7.4	-7.8	304.2
(+)-catechin	-7.5	-7.6	290.2
(-)-epicatechin	-7.5	-7.6	290.2
Ebselen	-6.6	-6.0	274.2

Reference

1. Wang, C.; Horby, P.W.; Hayden, F.G.; Gao, G.F. A novel coronavirus outbreak of global health concern. *Lancet* **2020**, *395*, 470-473, doi:10.1016/S0140-6736(20)30185-9.
2. Zhu, N.; Zhang, D.; Wang, W.; Li, X.; Yang, B.; Song, J.; Zhao, X.; Huang, B.; Shi, W.; Lu, R., et al. A Novel Coronavirus from Patients with Pneumonia in China, 2019. *N Engl J Med* **2020**, *382*, 727-733, doi:10.1056/NEJMoa2001017.
3. Ding, Q.; Lu, P.; Fan, Y.; Xia, Y.; Liu, M. The clinical characteristics of pneumonia patients coinfected with 2019 novel coronavirus and influenza virus in Wuhan, China. *J Med Virol* **2020**, 10.1002/jmv.25781, doi:10.1002/jmv.25781.
4. WHO. *Statement on the second meeting of the International Health Regulations (2005) Emergency Committee regarding the outbreak of novel coronavirus (2019-nCoV)*; World Health Organization: 2020.
5. WHO. Director-General's opening remarks at the media briefing on COVID-19-11 March 2020. **2020**.
6. Kim, J.H.; Marks, F.; Clemens, J.D. Looking beyond COVID-19 vaccine phase 3 trials. *Nature Medicine* **2021**, 10.1038/s41591-021-01230-y, doi:10.1038/s41591-021-01230-y.
7. Knoll, M.D.; Wonodi, C. Oxford-AstraZeneca COVID-19 vaccine efficacy. *The Lancet* **2021**, *397*, 72-74, doi:10.1016/S0140-6736(20)32623-4.
8. Painter, E.M.; Ussery, E.N.; Patel, A.; Hughes, M.M.; Zell, E.R.; Moulia, D.L.; Scharf, L.G.; Lynch, M.; Ritchey, M.D.; Toblin, R.L., et al. Demographic Characteristics of Persons Vaccinated During the First Month of the COVID-19 Vaccination Program — United States, December 14, 2020–January 14, 2021. *Morbidity and Mortality Weekly Report* **2021**, *70*,

507 174–177.

508 9. Dooling, K.; Marin, M.; Wallace, M.; McClung, N.; Chamberland, M.; Lee, G.M.; Talbot, H.K.;
509 Romero, J.R.; Bell, B.P.; Oliver, S.E. The Advisory Committee on Immunization Practices'
510 Updated Interim Recommendation for Allocation of COVID-19 Vaccine — United States,
511 December 2020. *Morbidity and Mortality Weekly Report* **2021**, *69*, 1657-1660.

512 10. CDC; FDA. Allergic Reactions Including Anaphylaxis After Receipt of the First Dose of
513 Moderna COVID-19 Vaccine — United States, December 21, 2020–January 10, 2021.
514 *Morbidity and Mortality Weekly Report* **2021**, *70*, 125–129.

515 11. Gharpure, R.; Guo, A.; Bishnoi, C.K.; Patel, U.; Gifford, D.; Tippins, A.; Jaffe, A.; Shulman, E.;
516 Stone, N.; Mungai, E., et al. Early COVID-19 First-Dose Vaccination Coverage Among
517 Residents and Staff Members of Skilled Nursing Facilities Participating in the Pharmacy
518 Partnership for Long-Term Care Program — United States, December 2020–January 2021.
519 *Morbidity and Mortality Weekly Report* **2021**, *70()*, 178–182.

520 12. McCarthy, K.R.; Rennick, L.J.; Nambulli, S.; Robinson-McCarthy, L.R.; Bain, W.G.; Haidar, G.;
521 Duprex, W.P. Natural deletions in the SARS-CoV-2 spike glycoprotein drive antibody escape.
522 *bioRxiv* **2020**, 10.1101/2020.11.19.389916, 2020.2011.2019.389916,
523 doi:10.1101/2020.11.19.389916.

524 13. Cohen, J. South Africa suspends use of AstraZeneca's COVID-19 vaccine after it fails to
525 clearly stop virus variant. *Science* 2021.

526 14. Kenilworth, N.J. Merck discontinues development of SARS-CoV2/COVID-19 vaccine
527 candidates; continues development of two investigational therapeutic candidates. *BUSINESS*
528 *WIRE* 2021.

529 15. Wang, M.; Cao, R.; Zhang, L.; Yang, X.; Liu, J.; Xu, M.; Shi, Z.; Hu, Z.; Zhong, W.; Xiao, G.
530 Remdesivir and chloroquine effectively inhibit the recently emerged novel coronavirus
531 (2019-nCoV) in vitro. *Cell Res* **2020**, *30*, 269-271, doi:10.1038/s41422-020-0282-0.
532 16. Bull-Otterson, L.; Gray, E.B.; Budnitz, D.S.; Strosnider, H.M.; Schieber, L.Z.; Courtney, J.;
533 García, M.C.; Brooks, J.T.; Kenzie, W.R.M.; Gundlapalli, A.V. Hydroxychloroquine and
534 Chloroquine Prescribing Patterns by Provider Specialty Following Initial Reports of Potential
535 Benefit for COVID-19 Treatment — United States, January–June 2020. *Morbidity and Mortality*
536 *Weekly Report* **2020**, *69*, 1210–1215.
537 17. Cao, B.; Wang, Y.; Wen, D.; Liu, W.; Wang, J.; Fan, G.; Ruan, L.; Song, B.; Cai, Y.; Wei, M., et
538 al. A Trial of Lopinavir-Ritonavir in Adults Hospitalized with Severe Covid-19. *N Engl J Med*
539 **2020**, *382*, 1787-1799, doi:10.1056/NEJMoa2001282.
540 18. Holshue, M.L.; DeBolt, C.; Lindquist, S.; Lofy, K.H.; Wiesman, J.; Bruce, H.; Spitters, C.;
541 Ericson, K.; Wilkerson, S.; Tural, A., et al. First Case of 2019 Novel Coronavirus in the United
542 States. *N Engl J Med* **2020**, *382*, 929-936, doi:10.1056/NEJMoa2001191.
543 19. Chen, Y.; Liu, Q.; Guo, D. Emerging coronaviruses: Genome structure, replication, and
544 pathogenesis. *J Med Virol* **2020**, 10.1002/jmv.26234, doi:10.1002/jmv.26234.
545 20. Hussain, S.; Pan, J.; Chen, Y.; Yang, Y.; Xu, J.; Peng, Y.; Wu, Y.; Li, Z.; Zhu, Y.; Tien, P., et al.
546 Identification of novel subgenomic RNAs and noncanonical transcription initiation signals of
547 severe acute respiratory syndrome coronavirus. *J Virol* **2005**, *79*, 5288-5295,
548 doi:10.1128/JVI.79.9.5288-5295.2005.
549 21. Ramajayam, R.; Tan, K.P.; Liang, P.H. Recent development of 3C and 3CL protease inhibitors
550 for anti-coronavirus and anti-picornavirus drug discovery. *Biochem Soc Trans* **2011**, *39*,

551 1371-1375, doi:10.1042/BST0391371.

552 22. Ren, Z.; Yan, L.; Zhang, N.; Guo, Y.; Yang, C.; Lou, Z.; Rao, Z. The newly emerged SARS-like
553 coronavirus HCoV-EMC also has an "Achilles' heel": current effective inhibitor targeting a
554 3C-like protease. *Protein Cell* **2013**, *4*, 248-250, doi:10.1007/s13238-013-2841-3.

555 23. Zhao, P.; Praissman, J.L.; Grant, O.C.; Cai, Y.; Xiao, T.; Rosenbalm, K.E.; Aoki, K.; Kellman,
556 B.P.; Bridger, R.; Barouch, D.H., et al. Virus-receptor interactions of glycosylated SARS-CoV-2
557 spike and human ACE2 receptor. *Cell Host Microbe* **2020**, *28*, 586-601.e586,
558 doi:10.1016/j.chom.2020.08.004.

559 24. Hoffmann, M.; Kleine-Weber, H.; Schroeder, S.; Krüger, N.; Herrler, T.; Erichsen, S.;
560 Schiergens, T.S.; Herrler, G.; Wu, N.-H.; Nitsche, A., et al. SARS-CoV-2 cell entry depends on
561 ACE2 and TMPRSS2 and is blocked by a clinically proven protease inhibitor. *Cell* **2020**, *181*,
562 271-280.e278, doi:https://doi.org/10.1016/j.cell.2020.02.052.

563 25. Yan, R.; Zhang, Y.; Li, Y.; Xia, L.; Guo, Y.; Zhou, Q. Structural basis for the recognition of
564 SARS-CoV-2 by full-length human ACE2. *Science* **2020**, *367*, 1444-1448,
565 doi:10.1126/science.abb2762.

566 26. Abdool Karim, S.S.; de Oliveira, T. New SARS-CoV-2 variants — Clinical, Public Health, and
567 Vaccine Implications. *New England Journal of Medicine* **2021**, *384*, 1866-1868,
568 doi:10.1056/NEJMc2100362.

569 27. Walensky, R.P.; Walke, H.T.; Fauci, A.S. SARS-CoV-2 Variants of Concern in the United
570 States—Challenges and Opportunities. *JAMA* **2021**, *325*, 1037-1038,
571 doi:10.1001/jama.2021.2294.

572 28. Fontanet, A.; Autran, B.; Lina, B.; Kieny, M.P.; Karim, S.S.A.; Sridhar, D. SARS-CoV-2

573 variants and ending the COVID-19 pandemic. *The Lancet* **2021**, *397*, 952-954,
574 doi:10.1016/S0140-6736(21)00370-6.
575 29. Altmann, D.M.; Boyton, R.J.; Beale, R. Immunity to SARS-CoV-2 variants of concern. *Science*
576 **2021**, *371*, 1103-1104, doi:10.1126/science.abg7404.
577 30. Petra, M.; Steven, K.; Mahesh Shanker, D.; Guido, P.; Bo, M.; Swapnil, M.; Charlie, W.;
578 Thomas, M.; Isabella, F.; Rawlings, D., et al. SARS-CoV-2 B.1.617.2 Delta variant emergence
579 and vaccine breakthrough. *Nature Portfolio* **2021**, 10.21203/rs.3.rs-637724/v1,
580 doi:10.21203/rs.3.rs-637724/v1.
581 31. Woo, P.C.Y.; Huang, Y.; Lau, S.K.P.; Yuen, K.-Y. Coronavirus genomics and bioinformatics
582 analysis. *Viruses* **2010**, *2*, 1804-1820.
583 32. Gaunt, E.R.; Hardie, A.; Claas, E.C.J.; Simmonds, P.; Templeton, K.E. Epidemiology and
584 clinical presentations of the four human coronaviruses 229E, HKU1, NL63, and OC43
585 detected over 3 years using a novel multiplex real-time PCR method. *J. Clin. Microbiol.* **2010**,
586 *48*, 2940-2947, doi:10.1128/jcm.00636-10.
587 33. Shirato, K.; Kanou, K.; Kawase, M.; Matsuyama, S. Clinical isolates of human coronavirus
588 229E bypass the endosome for cell entry. *Journal of Virology* **2017**, *91*, 12,
589 doi:10.1128/jvi.01387-16.
590 34. Farsani, S.M.J.; Dijkman, R.; Jebbink, M.F.; Goossens, H.; leven, M.; Deijs, M.; Molenkamp,
591 R.; van der Hoek, L. The first complete genome sequences of clinical isolates of human
592 coronavirus 229E. *Virus Genes* **2012**, *45*, 433-439, doi:10.1007/s11262-012-0807-9.
593 35. Fehr, A.R.; Perlman, S. Coronaviruses: An Overview of Their Replication and Pathogenesis. In
594 *Coronaviruses: Methods and Protocols*, Maier, H.J., Bickerton, E., Britton, P., Eds. Springer

595 New York: New York, NY, 2015; 10.1007/978-1-4939-2438-7_1pp. 1-23.

596 36. Shirato, K.; Kawase, M.; Watanabe, O.; Hirokawa, C.; Matsuyama, S.; Nishimura, H.; Taguchi,
597 F. Differences in neutralizing antigenicity between laboratory and clinical isolates of
598 HCoV-229E isolated in Japan in 2004-2008 depend on the S1 region sequence of the spike
599 protein. *J. Gen. Virol.* **2012**, *93*, 1908-1917, doi:10.1099/vir.0.043117-0.

600 37. Yang, H.; Xie, W.; Xue, X.; Yang, K.; Ma, J.; Liang, W.; Zhao, Q.; Zhou, Z.; Pei, D.; Ziebuhr, J.,
601 et al. Design of wide-spectrum inhibitors targeting coronavirus main proteases. *PLoS Biol*
602 **2005**, *3*, e324, doi:10.1371/journal.pbio.0030324.

603 38. Kim, Y.; Liu, H.; Galasiti Kankanamalage, A.C.; Weerasekara, S.; Hua, D.H.; Groutas, W.C.;
604 Chang, K.O.; Pedersen, N.C. Reversal of the Progression of Fatal Coronavirus Infection in
605 Cats by a Broad-Spectrum Coronavirus Protease Inhibitor. *PLoS Pathog* **2016**, *12*, e1005531,
606 doi:10.1371/journal.ppat.1005531.

607 39. Dai, W.; Zhang, B.; Jiang, X.M.; Su, H.; Li, J.; Zhao, Y.; Xie, X.; Jin, Z.; Peng, J.; Liu, F., et al.
608 Structure-based design of antiviral drug candidates targeting the SARS-CoV-2 main protease.
609 *Science* **2020**, *368*, 1331-1335, doi:10.1126/science.abb4489.

610 40. Jin, Z.; Du, X.; Xu, Y.; Deng, Y.; Liu, M.; Zhao, Y.; Zhang, B.; Li, X.; Zhang, L.; Peng, C., et al.
611 Structure of M(pro) from SARS-CoV-2 and discovery of its inhibitors. *Nature* **2020**, *582*,
612 289-293, doi:10.1038/s41586-020-2223-y.

613 41. Ye, G.; Wang, X.; Tong, X.; Shi, Y.; Fu, Z.F.; Peng, G. Structural Basis for Inhibiting Porcine
614 Epidemic Diarrhea Virus Replication with the 3C-Like Protease Inhibitor GC376. *Viruses* **2020**,
615 *12*, doi:10.3390/v12020240.

616 42. Chen, L.; Gui, C.; Luo, X.; Yang, Q.; Gunther, S.; Scandella, E.; Drosten, C.; Bai, D.; He, X.;

617 Ludewig, B., et al. Cinanserin is an inhibitor of the 3C-like proteinase of severe acute
618 respiratory syndrome coronavirus and strongly reduces virus replication in vitro. *J Virol* **2005**,
619 *79*, 7095-7103, doi:10.1128/JVI.79.11.7095-7103.2005.
620 43. Zhang, L.; Liu, Y. Potential interventions for novel coronavirus in China: A systematic review. *J*
621 *Med Virol* **2020**, *92*, 479-490, doi:10.1002/jmv.25707.
622 44. Zhu, Y.; Xie, D.-Y. Docking characterization and in vitro inhibitory activity of flavan-3-ols and
623 dimeric proanthocyanidins against the main protease activity of SARS-Cov-2. *Front. Plant Sci.*
624 **2020**, *11*, doi:10.3389/fpls.2020.601316.
625 45. Fowler, Z.L.; Koffas, M.A. Biosynthesis and biotechnological production of flavanones: current
626 state and perspectives. *Appl Microbiol Biotechnol* **2009**, *83*, 799-808,
627 doi:10.1007/s00253-009-2039-z.
628 46. Hostetler, G.L.; Ralston, R.A.; Schwartz, S.J. Flavones: Food Sources, Bioavailability,
629 Metabolism, and Bioactivity. *Adv Nutr* **2017**, *8*, 423-435, doi:10.3945/an.116.012948.
630 47. Xie, D.-Y.; Jackson, L.A.; Cooper, J.D.; Ferreira, D.; Paiva, N.L. Molecular and biochemical
631 analysis of two cDNA clones encoding dihydroflavonol-4-reductase from *Medicago truncatula*.
632 *Plant Physiol* **2004**, *134*, 979-994, doi:10.1104/pp.103.030221.
633 48. Xie, D.-Y.; Dixon, R.A. Proanthocyanidin biosynthesis - still more questions than answers?
634 *Phytochemistry* **2005**, *66*, 2127-2144.
635 49. Moon, J.H.; Tsushida, T.; Nakahara, K.; Terao, J. Identification of quercetin
636 3-O-beta-D-glucuronide as an antioxidative metabolite in rat plasma after oral administration of
637 quercetin. *Free Radic. Biol. Med.* **2001**, *30*, 1274-1285, doi:10.1016/s0891-5849(01)00522-6.
638 50. Murota, K.; Terao, J. Antioxidative flavonoid quercetin: implication of its intestinal absorption

639 and metabolism. *Archives of Biochemistry an Biophysics* **2003**, *417*, 12-17.

640 51. Egert, S.; Wolffram, S.; Bosy-Westphal, A.; Boesch-Saadatmandi, C.; Wagner, A.E.; Frank, J.;
641 Rimbach, G.; Mueller, M.J. Daily quercetin supplementation dose-dependently increases
642 plasma quercetin concentrations in healthy humans. *J. Nutr.* **2008**, *138*, 1615-1621.

643 52. Chopra, M.; Fitzsimons, P.E.E.; Strain, J.J.T.; Thurnham, D.I.; Howard, A.N. Nonalcoholic red
644 wine extract and quercetin inhibit LDL oxidation without affecting plasma antioxidant vitamin
645 and carotenoid concentrations. *Clin. Chem.* **2000**, *46*, 1162-1170.

646 53. Hertog, M.G.L.; Feskens, E.J.M.; Hollman, P.C.H.; Katan, M.B.; Kromhout, D. Dietary
647 antioxidant flavonols and risk of coronary heart disease- the Zutphen elderly study. *Lancet*
648 **1993**, *342*, 1007-1011.

649 54. de Vries, J.H.M.; Hollman, P.C.H.; Meyboom, S.; Buysman, M.; Zock, P.L.; van Staveren,
650 W.A.; Katan, M.B. Plasma concentrations and urinary excretion of the antioxidant flavonols
651 quercetin and kaempferol as biomarkers for dietary intake. *Am. J. Clin. Nutr.* **1998**, *68*, 60-65.

652 55. Kolhir, V.K.; Bykov, V.A.; Baginskaja, A.I.; Sokolov, S.Y.; Glazova, N.G.; Leskova, T.E.;
653 Sakovich, G.S.; Tjukavkina, N.A.; Kolesnik, Y.A.; Rulenko, I.A. Antioxidant activity of a
654 dihydroquercetin isolated from Larix gmelinii (Rupr) Rupr wood. *Phytother. Res.* **1996**, *10*,
655 478-482.

656 56. Teselkin, Y.O.; Babenkova, I.V.; Tjukavkina, N.A.; Rulenko, I.A.; Kolesnik, Y.A.; Kolhir, V.K.;
657 Eichholz, A.A. Influence of dihydroquercetin on the lipid peroxidation of mice during
658 post-radiation period. *Phytother. Res.* **1998**, *12*, 517-519,
659 doi:10.1002/(sici)1099-1573(199811)12:7<517::Aid-ptr342>3.0.Co;2-d.

660 57. Teselkin, Y.O.; Babenkova, I.V.; Kolhir, V.K.; Baginskaya, A.I.; Tjukavkina, N.A.; Kolesnik,

661 Y.A.; Selivanova, I.A.; Eichholz, A.A. Dihydroquercetin as a means of antioxidative defence in
662 rats with tetrachloromethane hepatitis. *Phytother. Res.* **2000**, *14*, 160-162,
663 doi:10.1002/(sici)1099-1573(200005)14:3<160::Aid-ptr555>3.0.Co;2-y.
664 58. Weidmann, A.E. Dihydroquercetin: More than just an impurity? *Eur. J. Pharmacol.* **2012**, *684*,
665 19-26, doi:10.1016/j.ejphar.2012.03.035.
666 59. Mehrbod, P.; Hudy, D.; Shyntum, D.; Markowski, J.; Los, M.J.; Ghavami, S. Quercetin as a
667 natural therapeutic candidate for the treatment of influenza virus. *Biomolecules* **2021**, *11*, 29,
668 doi:10.3390/biom11010010.
669 60. dos Santos, A.E.; Kuster, R.M.; Yamamoto, K.A.; Salles, T.S.; Campos, R.; de Meneses,
670 M.D.F.; Soares, M.R.; Ferreira, D. Quercetin and quercetin 3-O-glycosides from Bauhinia
671 longifolia (Bong.) Steud. show anti-Mayaro virus activity. *Parasites Vectors* **2014**, *7*, 7,
672 doi:10.1186/1756-3305-7-130.
673 61. Cheng, Z.K.; Sun, G.; Guo, W.; Huang, Y.Y.; Sun, W.H.; Zhao, F.; Hu, K.H. Inhibition of
674 hepatitis B virus replication by quercetin in human hepatoma cell lines. *Virol. Sin.* **2015**, *30*,
675 261-268, doi:10.1007/s12250-015-3584-5.
676 62. Nakabayashi, H.; Taketa, K.; Yamane, T.; Miyazaki, M.; Miyano, K.; Sato, J. Phenotypical
677 stability of a human hepatoma-cell line, Huh-7, in long-term culture with chemically defined
678 medium. *Gann* **1984**, *75*, 151-158.
679 63. Shih, C.M.; Lo, S.C.J.; Miyamura, T.; Chen, S.Y.; Lee, Y.H.W. Suppression of hepatitis-B virus
680 expression and replication by hepatitis-C virus core protein in Huh-7 cells. *Journal of Virology*
681 **1993**, *67*, 5823-5832, doi:10.1128/jvi.67.10.5823-5832.1993.
682 64. Dewi, B.E.; Desti, H.; Ratningpoeti, E.; Sudiro, M.; Fithriyah; Angelina, M.; Iop. Effectivity of

683 quercetin as antiviral to dengue virus-2 strain New Guinea C in Huh 7-it 1 cell line. In *3rd*
684 *International Conference on Natural Products and Bioresource Sciences*, Iop Publishing Ltd:
685 Bristol, 2020; Vol. 462.
686 65. Thongsri, P.; Sa-ngiamsuntorn, K.; Sithisarn, P.; Chomnawang, M.T.; Thirapanmethee, K.
687 Cladogynos orientalis Zipp. extracts inhibit cell culture-derived hepatitis C virus genotype 2a
688 replication in Huh-7 cells through NS5B inhibition. *Asian Pac. Trop. Biomed.* **2019**, *9*, 346-352,
689 doi:10.4103/2221-1691.262079.
690 66. Logue, J.; Licona, W.V.; Cooper, T.K.; Reeder, B.; Byrum, R.; Qin, J.; Murphy, N.D.; Cong, Y.;
691 Bonilla, A.; Sword, J., et al. Ebola virus isolation using Huh-7 cells has methodological
692 advantages and similar sensitivity to isolation using other cell types and suckling BALB/c
693 laboratory mice. *Viruses-Basel* **2019**, *11*, 14, doi:10.3390/v11020161.
694 67. Bucknall, R.A.; Chanock, R.M.; Kapikian, A.Z.; King, L.M. Studies with human coronaviruses.
695 2. Some properties of strains 229E and OC43. *Proc. Soc. Exp. Biol. Med.* **1972**, *139*, 722-&.
696 68. Kennedy, D.A.; Johnsonlussenburg, C.M. Isolation and morphology of internal component of
697 human coronavirus, strain 229E. *Intervirology* **1976**, *6*, 197-206.
698 69. Hierholzer, J.C. Purification and biophysical properties of human coronavirus 229E. *Virology*
699 **1976**, *75*, 155-165, doi:10.1016/0042-6822(76)90014-3.
700 70. Macnaughton, M.R.; Madge, M.H. Genome of human coronavirus strain 229E. *J. Gen. Virol.*
701 **1978**, *39*, 497-504, doi:10.1099/0022-1317-39-3-497.
702 71. Friedman, N.; Jacob-Hirsch, J.; Drori, Y.; Eran, E.; Kol, N.; Nayshool, O.; Mendelson, E.;
703 Rechavi, G.; Mandelboim, M. Transcriptomic profiling and genomic mutational analysis of
704 Human coronavirus (HCoV)-229E-infected human cells. *PLoS One* **2021**, *16*, 15,

705 doi:10.1371/journal.pone.0247128.

706 72. Ziebuhr, J.; Heusipp, G.; Siddell, S.G. Biosynthesis, purification, and characterization of the
707 human coronavirus 229E 3C-like proteinase. *Journal of Virology* **1997**, *71*, 3992-3997,
708 doi:10.1128/jvi.71.5.3992-3997.1997.

709 73. Ziebuhr, J.; Herold, J.; Siddell, S.G. Characterization of a human coronavius (strain 229E)
710 3C-like proteinase activity. *Journal of Virology* **1995**, *69*, 4331-4338,
711 doi:10.1128/jvi.69.7.4331-4338.1995.

712 74. Ziebuhr, J.; Heusipp, G.; Seybert, A.; Siddell, S.G. Substrate specificity of the human
713 coronavirus 229E 3C-like proteinase. In *Coronaviruses and Arteriviruses*, Enjuanes, L., Siddell,
714 S.G., Spaan, W., Eds. Plenum Press Div Plenum Publishing Corp: New York, 1998; Vol. 440,
715 pp. 115-120.

716 75. Prior, A.M.; Kim, Y.J.; Weerasekara, S.; Moroze, M.; Alliston, K.R.; Uy, R.A.Z.; Groutas, W.C.;
717 Chang, K.O.; Hua, D.H. Design, synthesis, and bioevaluation of viral 3C and 3C-like protease
718 inhibitors. *Bioorg. Med. Chem. Lett.* **2013**, *23*, 6317-6320, doi:10.1016/j.bmcl.2013.09.070.

719 76. Chuck, C.P.; Chen, C.; Ke, Z.H.; Wan, D.C.C.; Chow, H.F.; Wong, K.B. Design, synthesis and
720 crystallographic analysis of nitrile-based broad-spectrum peptidomimetic inhibitors for
721 coronavirus 3C-like proteases. *Eur. J. Med. Chem.* **2013**, *59*, 1-6,
722 doi:10.1016/j.ejmech.2012.10.053.

723 77. Lee, C.C.; Kuo, C.J.; Ko, T.P.; Hsu, M.F.; Tsui, Y.C.; Chang, S.C.; Yang, S.; Chen, S.J.; Chen,
724 H.C.; Hsu, M.C., et al. Structural Basis of Inhibition Specificities of 3C and 3C-like Proteases
725 by Zinc-coordinating and Peptidomimetic Compounds. *J. Biol. Chem.* **2009**, *284*, 7646-7655,
726 doi:10.1074/jbc.M807947200.

78. Barrett, P.N.; Meyer, H.; Wachtel, I.; Eibl, J.; Dorner, F. Determination of the inactivation kinetics of hepatitis A virus in human plasma products using a simple TCID50 assay. *J. Med. Virol.* **1996**, *49*, 1-6, doi:10.1002/(sici)1096-9071(199605)49:1<1::Aid-jmv1>3.0.Co;2-a.

79. Kärber, G. Beitrag zur kollektiven Behandlung pharmakologischer Reihenversuche. *Naunyn-Schmiedebergs Archiv für experimentelle Pathologie und Pharmakologie* **1931**, *162*, 480-483, doi:10.1007/BF01863914.

80. Spearman, C. THe method of 'Right and Wrong Cases' ('Constant stiumuli') without Gauss's formulae. *Br. J. Psychol.* **1908**, *2*, 227-242, doi:10.1111/j.2044-8295.1908.tb00176.x.

81. Parvez, M.K.; Al-Dosari, M.S.; Arbab, A.H.; Al-Rehaily, A.J.; Abdelwahid, M.A.S. Bioassay-guided isolation of anti-hepatitis B virus flavonoid myricetin-3-O-rhamnoside along with quercetin from Guiera senegalensis leaves. *Saudi Pharm. J.* **2020**, *28*, 550-559, doi:10.1016/j.jsps.2020.03.006.

82. Wong, G.; He, S.H.; Siragam, V.; Bi, Y.H.; Mbikay, M.; Chretien, M.; Qiu, X.G. Antiviral activity of quercetin-3-beta-O-D-glucoside against Zika virus infection. *Virol. Sin.* **2017**, *32*, 545-547, doi:10.1007/s12250-017-4057-9.

83. Qiu, X.G.; Kroeker, A.; He, S.H.; Kozak, R.; Audet, J.; Mbikay, M.; Chretienc, M. Prophylactic Efficacy of Quercetin 3-beta-O-D-Glucoside against Ebola Virus Infection. *Antimicrob. Agents Chemother.* **2016**, *60*, 5182-5188, doi:10.1128/aac.00307-16.

84. Xu, Z.; Li, X.Q.; Yang, H.; Poolsawat, L.; Wang, P.; Leng, X.J. Dietary rutin promoted the growth, serum antioxidant response and flesh collagen, free amino acids contents of grass carp (Ctenopharyngodon idella). *Aquac. Nutr.* **2021**, *27*, 544-555, doi:10.1111/anu.13205.

85. Ragheb, S.R.; El Wakeel, L.M.; Nasr, M.S.; Sabri, N.A. Impact of rutin and vitamin C

749 combination on oxidative stress and glycemic control in patients with type 2 diabetes. *Clin.*
750 *Nutr. ESPEN* **2020**, *35*, 128-135, doi:10.1016/j.clnesp.2019.10.015.
751 86. da Silva, E.R.; Brogi, S.; Lucon, J.F.; Campiani, G.; Gemma, S.; Maquiaveli, C.D. Dietary
752 polyphenols rutin, taxifolin and quercetin related compounds target Leishmania amazonensis
753 arginase. *Food Funct.* **2019**, *10*, 3172-3180, doi:10.1039/c9fo00265k.
754 87. Kolarevic, A.; Pavlovic, A.; Djordjevic, A.; Lazarevic, J.; Savic, S.; Kocic, G.; Anderluh, M.;
755 Smelcerovic, A. Rutin as Deoxyribonuclease I Inhibitor. *Chem. Biodivers.* **2019**, *16*, 9,
756 doi:10.1002/cbdv.201900069.
757 88. Seifert, J. *Role of Quercetin in Sports Nutrition*; Elsevier Academic Press Inc: San Diego, 2013;
758 10.1016/b978-0-12-396454-0.00052-7pp. 497-500.
759 89. Amanzadeh, E.; Esmaeili, A.; Rahgozar, S.; Nourbakhshnia, M. Application of quercetin in
760 neurological disorders: from nutrition to nanomedicine. *Rev. Neurosci.* **2019**, *30*, 555-572,
761 doi:10.1515/revneuro-2018-0080.
762 90. Burak, C.; Brull, V.; Langguth, P.; Zimmermann, B.F.; Stoffel-Wagner, B.; Sausen, U.; Stehle,
763 P.; Wolffram, S.; Egert, S. Higher plasma quercetin levels following oral administration of an
764 onion skin extract compared with pure quercetin dihydrate in humans. *Eur. J. Nutr.* **2017**, *56*,
765 343-353, doi:10.1007/s00394-015-1084-x.
766 91. Egert, S.; Wolffram, S.; Schulze, B.; Langguth, P.; Hubbermann, E.M.; Schwarz, K.; Adolphi,
767 B.; Bosy-Westphal, A.; Rimbach, G.; Muller, M.J. Enriched cereal bars are more effective in
768 increasing plasma quercetin compared with quercetin from powder-filled hard capsules. *Br. J.*
769 *Nutr.* **2012**, *107*, 539-546, doi:10.1017/s0007114511003242.
770 92. Careri, M.; Corradini, C.; Elviri, L.; Nicoletti, I.; Zagnoni, I. Direct HPLC analysis of quercetin

771 and trans-resveratrol in red wine, grape, and winemaking byproducts. *J Agric Food Chem*
772 **2003**, *51*, 5226-5231.
773 93. Meng, X.F.; Maliakal, P.; Lu, H.; Lee, M.J.; Yang, C.S. Urinary and plasma levels of resveratrol
774 and quercetin in humans, mice, and rats after ingestion of pure compounds and grape juice. *J.*
775 *Agric. Food Chem.* **2004**, *52*, 935-942, doi:10.1021/jf030582e.
776 94. Erlund, I.; Silaste, M.L.; Alfthan, G.; Rantala, M.; Kesaniemi, Y.A.; Aro, A. Plasma
777 concentrations of the flavonoids hesperetin, naringenin and quercetin in human subjects
778 following their habitual diets, and diets high or low in fruit and vegetables. *Eur. J. Clin. Nutr.*
779 **2002**, *56*, 891-898, doi:10.1038/sj.ejcn.1601409.
780 95. Snyder, S.M.; Zhao, B.X.; Luo, T.; Kaiser, C.; Cavender, G.; Hamilton-Reeves, J.; Sullivan,
781 D.K.; Shay, N.F. Consumption of Quercetin and Quercetin-Containing Apple and Cherry
782 Extracts Affects Blood Glucose Concentration, Hepatic Metabolism, and Gene Expression
783 Patterns in Obese C57BL/6J High Fat-Fed Mice. *J. Nutr.* **2016**, *146*, 1001-1007,
784 doi:10.3945/jn.115.228817.
785 96. Day, A.J.; Williamson, G. Biomarkers for exposure to dietary flavonoids: a review of the current
786 evidence for identification of quercetin glycosides in plasma. *Br. J. Nutr.* **2001**, *86*, S105-S110,
787 doi:10.1079/bjn2001342.
788 97. Shi, Y.L.; Williamson, G. Quercetin lowers plasma uric acid in pre-hyperuricaemic males: a
789 randomised, double-blinded, placebo-controlled, cross-over trial. *Br. J. Nutr.* **2016**, *115*,
790 800-806, doi:10.1017/s0007114515005310.
791 98. Mohammadi-Sartang, M.; Mazloom, Z.; Sherafatmanesh, S.; Ghorbani, M.; Firoozi, D. Effects
792 of supplementation with quercetin on plasma C-reactive protein concentrations: a systematic

793 review and meta-analysis of randomized controlled trials. *Eur. J. Clin. Nutr.* **2017**, *71*,
794 1033-1039, doi:10.1038/ejcn.2017.55.
795 99. Huang, H.H.; Liao, D.; Dong, Y.; Pu, R. Effect of quercetin supplementation on plasma lipid
796 profiles, blood pressure, and glucose levels: a systematic review and meta-analysis. *Nutr. Rev.*
797 **2020**, *78*, 615-626, doi:10.1093/nutrit/nuz071.
798 100. Olthof, M.R.; Hollman, P.C.; Vree, T.B.; Katan, M.B. Bioavailabilities of quercetin-3-glucoside
799 and quercetin-4'-glucoside do not differ in humans. *J Nutr* **2000**, *130*, 1200-1203,
800 doi:10.1093/jn/130.5.1200.
801 101. de Whalley, C.V.; Rankin, S.M.; Hoult, J.R.; Jessup, W.; Leake, D.S. Flavonoids inhibit the
802 oxidative modification of low density lipoproteins by macrophages. *Biochem Pharmacol* **1990**,
803 *39*, 1743-1750, doi:10.1016/0006-2952(90)90120-a.
804 102. Justino, G.; Santos, M.; Mira, L. Plasma metabolites of quercetin and their antioxidant potential.
805 *Free Radic. Biol. Med.* **2002**, *33*, S203-S203.
806 103. Terao, J.; Yamaguchi, S.; Shirai, M.; Miyoshi, M.; Moon, J.H.; Oshima, S.; Inakuma, T.;
807 Tsushida, T.; Kato, Y. Protection by quercetin and quercetin 3-O-beta-glueuronide of
808 peroxynitrite-induced antioxidant consumption in human plasma low-density lipoprotein. *Free*
809 *Radic. Res.* **2001**, *35*, 925-931, doi:10.1080/10715760100301421.
810 104. Hertog, M.G.; Feskens, E.J.; Hollman, P.C.; Katan, M.B.; Kromhout, D. Dietary antioxidant
811 flavonoids and risk of coronary heart disease: the Zutphen Elderly Study. *Lancet* **1993**, *342*,
812 1007-1011, doi:10.1016/0140-6736(93)92876-u.
813 105. Manach, C.; Morand, C.; Crespy, V.; Demigne, C.; Texier, O.; Regerat, F.; Remesy, C.
814 Quercetin is recovered in human plasma as conjugated derivatives which retain antioxidant

815 properties. *FEBS Lett.* **1998**, *426*, 331-336, doi:10.1016/s0014-5793(98)00367-6.

816 106. Sato, S.; Mukai, Y. Modulation of chronic inflammation by quercetin: The beneficial effects on

817 obesity. *J. Inflamm. Res.* **2020**, *13*, 421-431, doi:10.2147/jir.S228361.

818 107. Carullo, G.; Cappello, A.R.; Frattaruolo, L.; Badolato, M.; Armentano, B.; Aiello, F. Quercetin

819 and derivatives: useful tools in inflammation and pain management. *Future Med. Chem.* **2017**,

820 *9*, 79-93, doi:10.4155/fmc-2016-0186.

821 108. Tejada, S.; Nabavi, S.M.; Capo, X.; Martorell, M.; Bibiloni, M.D.; Tur, J.A.; Pons, A.; Sureda, A.

822 Quercetin effects on exercise induced oxidative stress and inflammation. *Curr. Org. Chem.*

823 **2017**, *21*, 348-356, doi:10.2174/1385272820666161017122202.

824 109. Li, Y.; Yao, J.Y.; Han, C.Y.; Yang, J.X.; Chaudhry, M.T.; Wang, S.N.; Liu, H.N.; Yin, Y.L.

825 Quercetin, Inflammation and Immunity. *Nutrients* **2016**, *8*, 14, doi:10.3390/nu8030167.

826 110. Chen, S.; Jiang, H.M.; Wu, X.S.; Fang, J. Therapeutic Effects of Quercetin on Inflammation,

827 Obesity, and Type 2 Diabetes. *Mediat. Inflamm.* **2016**, *2016*, 5, doi:10.1155/2016/9340637.

828

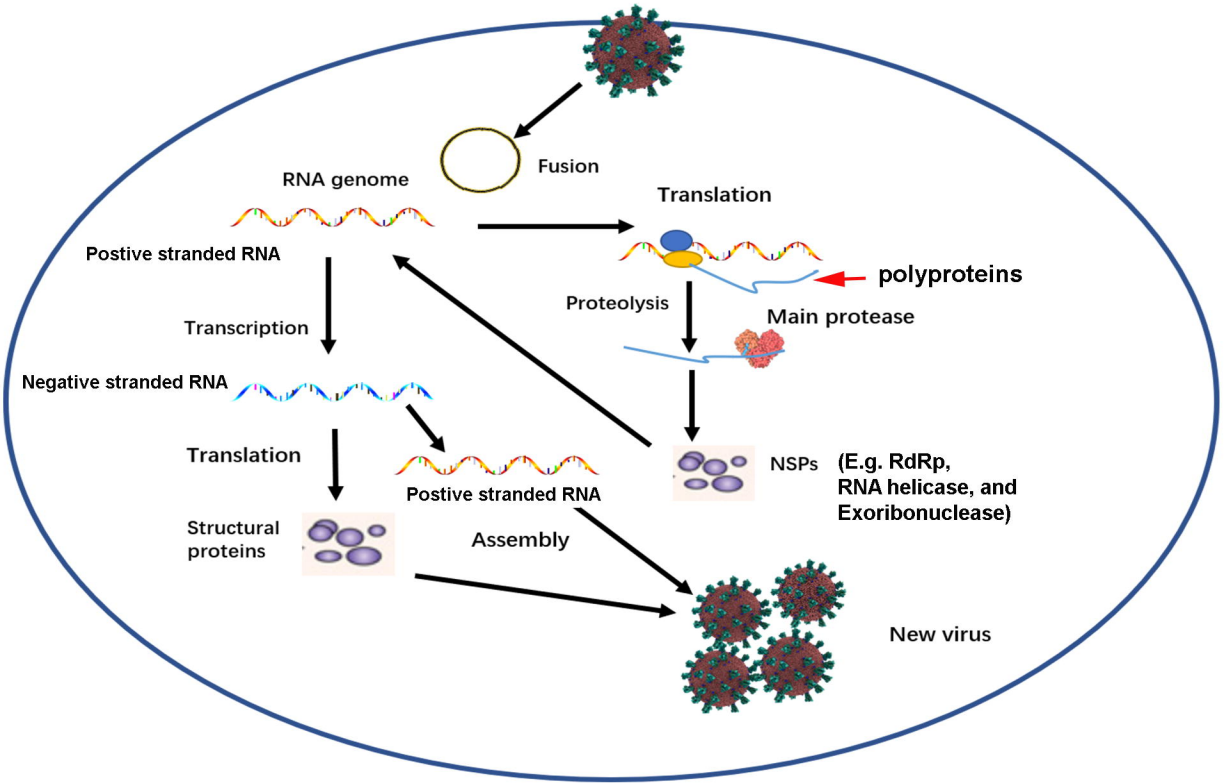
Fusion
RNA genome
Translation
Postive stranded RNA
polyproteins
Proteolysis
Main protease
Transcription
Negative stranded RNA
Translation
Postive stranded RNA
NSPs
(E.g. RdRp,
RNA helicase, and
Exoribonuclease)
Structural
proteins
Assembly
New virus

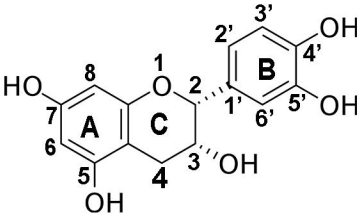

(-)-Epicatachin

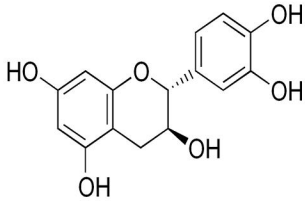

(+)-Catechin

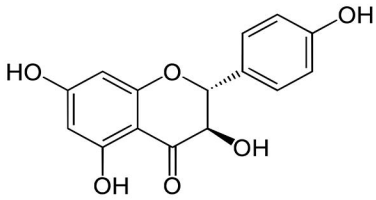

(+)-Dihydrokaempferol (DHK)

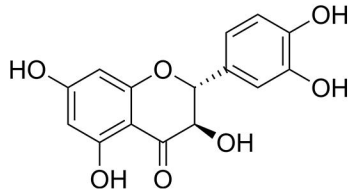

(+)- Dihydroquercetin (DHQ)

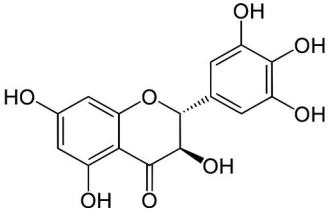

(+)-Dihydromyricetin (DHM)

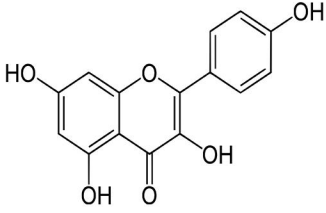

Kaempferol

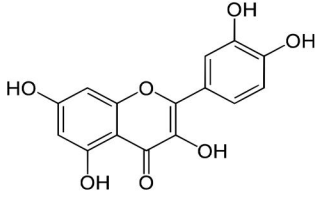

Quercetin

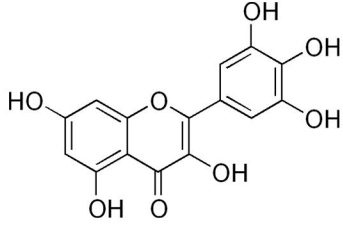

Myricetin

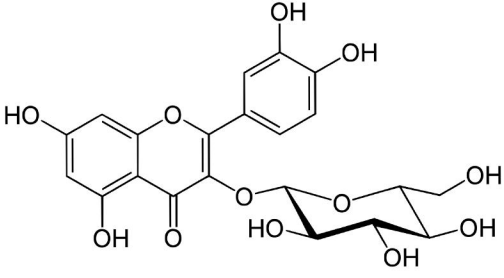

Quercetin-3-O-glycoside

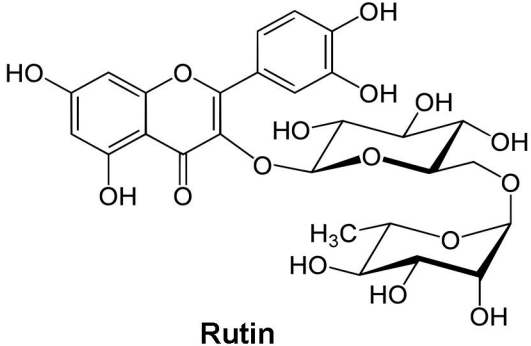

Rutin

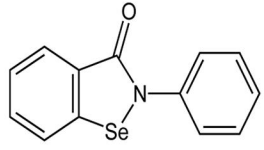

Ebselen

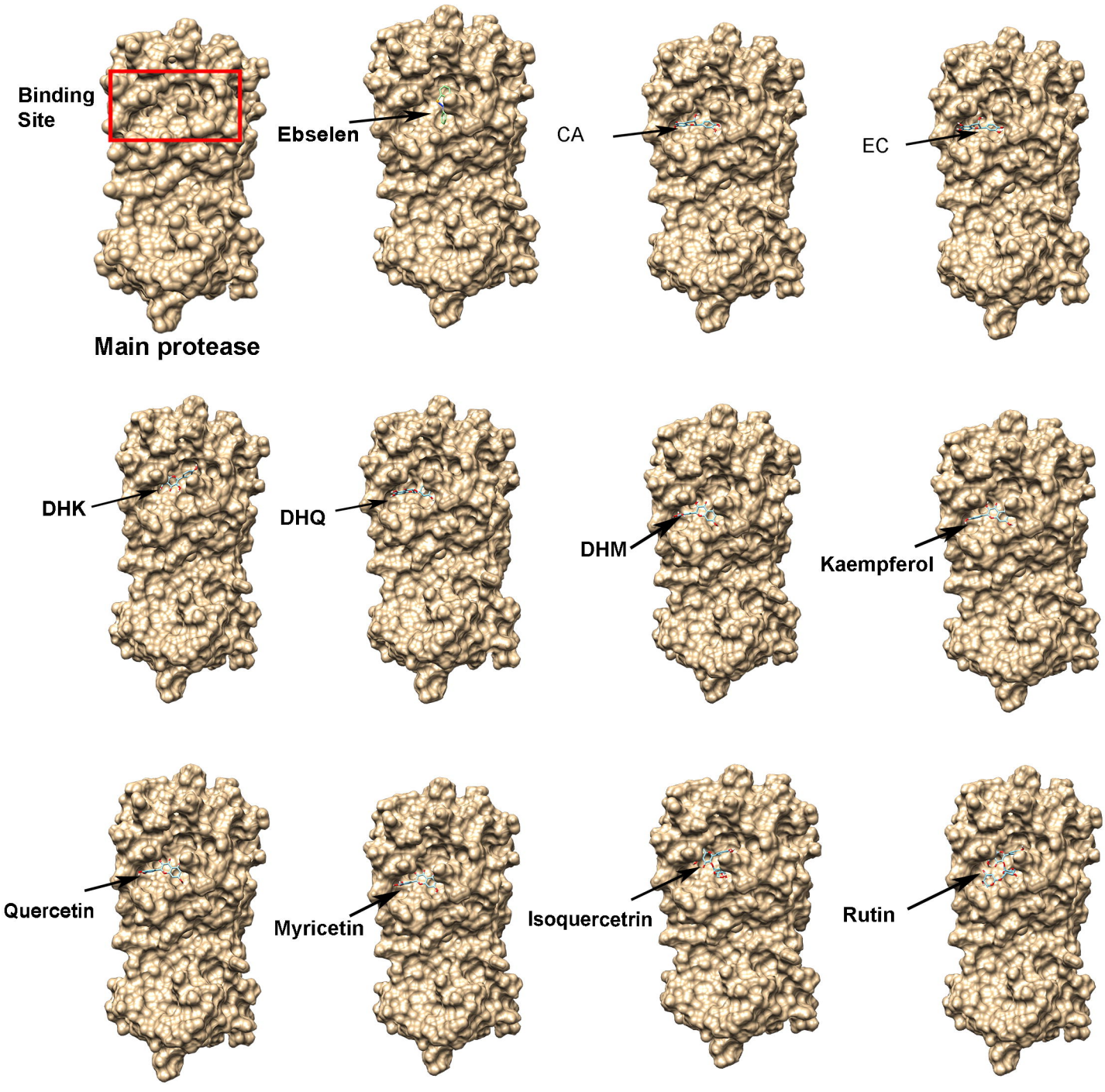
Binding Site
Main protease
Ebselen
CA
EC
DHK
DHQ
DHM
Kaempferol
Quercetin
Myricetin
Isoquercetrin
Rutin

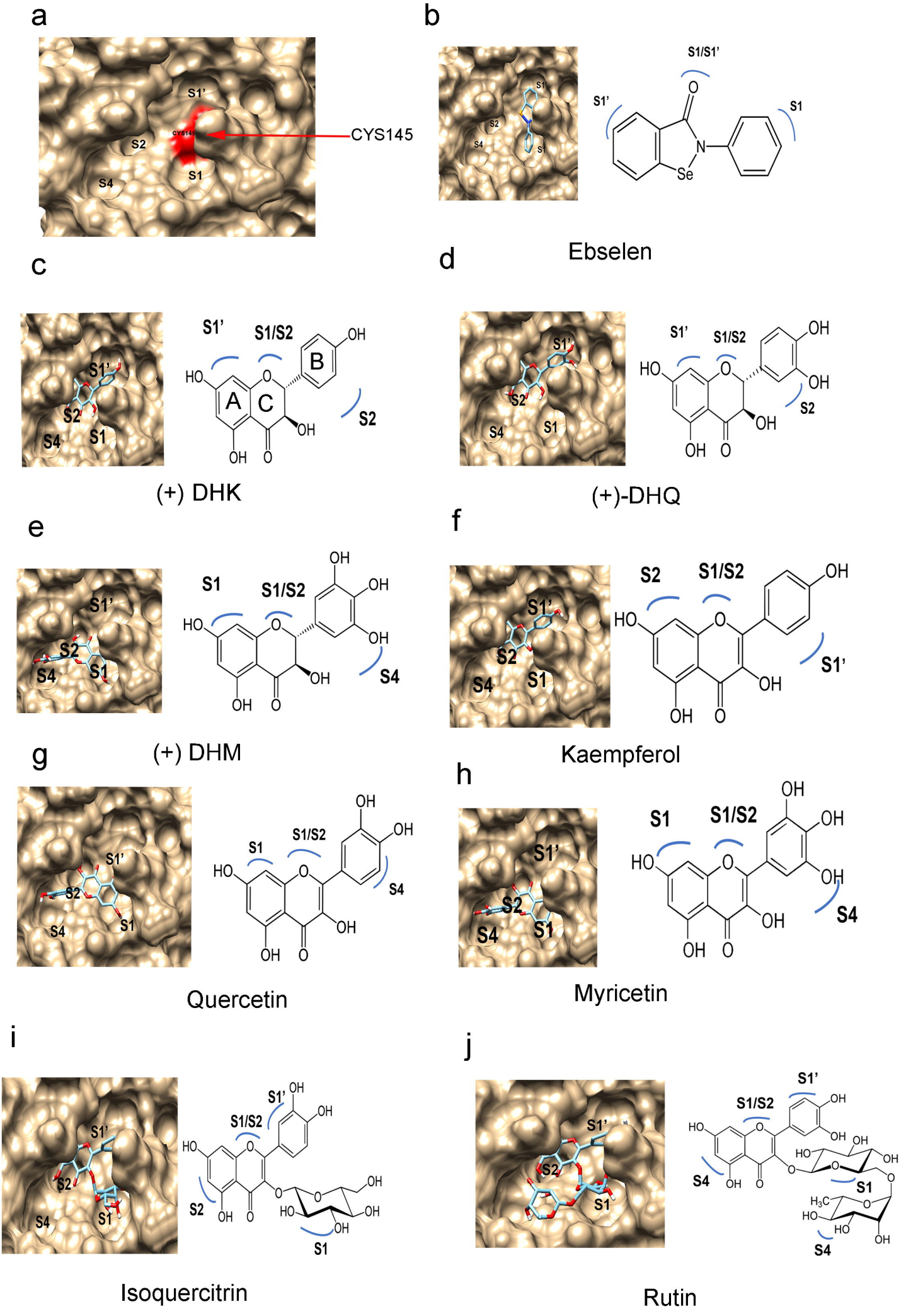
a
S1'
S2
S4
S1
CYS145
b
S1/S1'
S1'
S1
O
N
Se
Ebselen
c
S1'
S1/S2
S2
S4
S1
A
B
C
HO
OH
O
(+) DHK
d
S1'
S1/S2
S2
S4
S1
HO
OH
O
(+)-DHQ
e
S1
S1/S2
S1'
S2
S4
S1
HO
OH
O
(+) DHM
f
S2
S1/S2
S1'
S2
S4
S1
HO
OH
O
Kaempferol
g
S1
S1/S2
S1'
S2
S4
S1
HO
OH
O
Quercetin
h
S1
S1/S2
S1'
S2
S4
S1
HO
OH
O
Myricetin
i
S1'
S1/S2
S1'
S2
S4
S1
HO
OH
O
Isoquercitrin
j
S1'
S1/S2
S1'
S2
S1
S4
S1
S4
HO
OH
O
Rutin

a

```
hCov-229E     AGLRKMAQPSGFVEKCVVRVCYGNTVLNGLWLGDIVYCPRHVIASNTTS-AIDYDHEYSI   59
SARS-Cov-2    SGFRKMAFPSGKVEGCMVQVTCGTTTLNGLWLDDVVYCPRHVICTSEDMLNPNYEDLLIR   60
              :*:**** *** ** *:*:*  *.*.******.*:*******.:.       :*:.

hCov-229E     MRLHNFSIISGTAFLGVVGATMHGVTLKIKVSQTNMHTPRHSFRTLKSGEGFNILACYDG   119
SARS-Cov-2    KSNHNFLVQAGNVQLRVIGHSMQNCVLKLKVDTANPKTPKYKFVRIQPGQTFSVLACYNG   120
                 *** : :*.. * *:* :*:. .**:**. :* :**::.*  :: *: *.:****:*

hCov-229E     CAQGVFGVNMRTNWTIRGSFINAACGSPGYNLKNGEVEFVYMHQIELGSGSHVGSSFDGV   179
SARS-Cov-2    SPSGVYQCAMRPNFTIKGSFLNGSCGSVGFNIDYDCVSFCYMHHMELPTGVHAGTDLEGN   180
              . .**:   ** *:**:***:*:*:*** *:*:. . *.* ***::** :* *.*:.::*

hCov-229E     MYGGFEDQPNLQVESANQMLTVNVVAFLYAAILNGCTWWLKGEKLFVEHYNEWAQANGFT   239
SARS-Cov-2    FYGPFVDRQTAQAAGTDTTITVNVLAWLYAAVINGDRWFLNRFTTTLNDFNLVAMKYNYE   240
              :** * *: . *. .::  :****:*:****::**  *:*:  .  ::.:*  *   .:

hCov-229E     AMNG--EDAFSILAAKTGVCVERLL-HAIQVLNNGFGGKQILGYSSLNDEFSINEVVKQM   296
SARS-Cov-2    PLTQDHVDILGPLSAQTGIAVLDMCASLKELLQNGMNGRTILGSALLEDEFTPFDVVRQC   300
               :.    * :. *:*:**:.*  :     ::*:**:.*: *** : *:***:  :**:*

hCov-229E     FGVNLQ  302
SARS-Cov-2    SGVTFQ  306
               **.:*
```

b

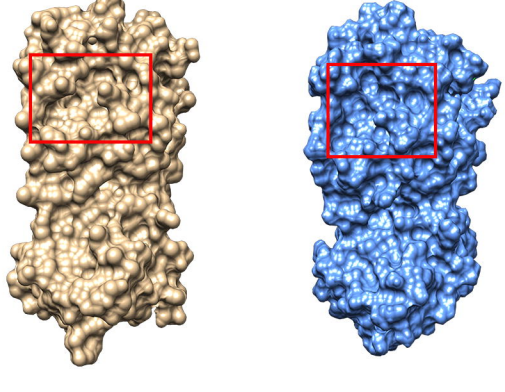

c

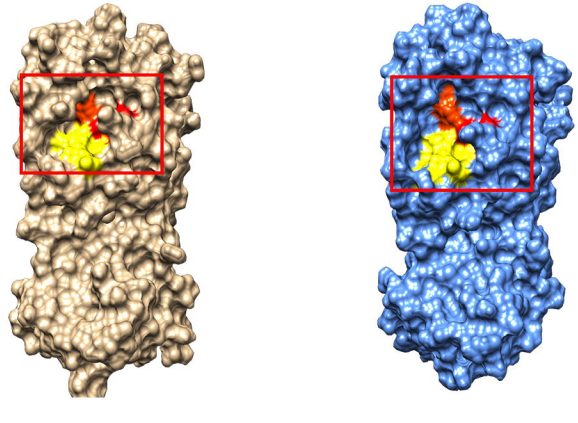

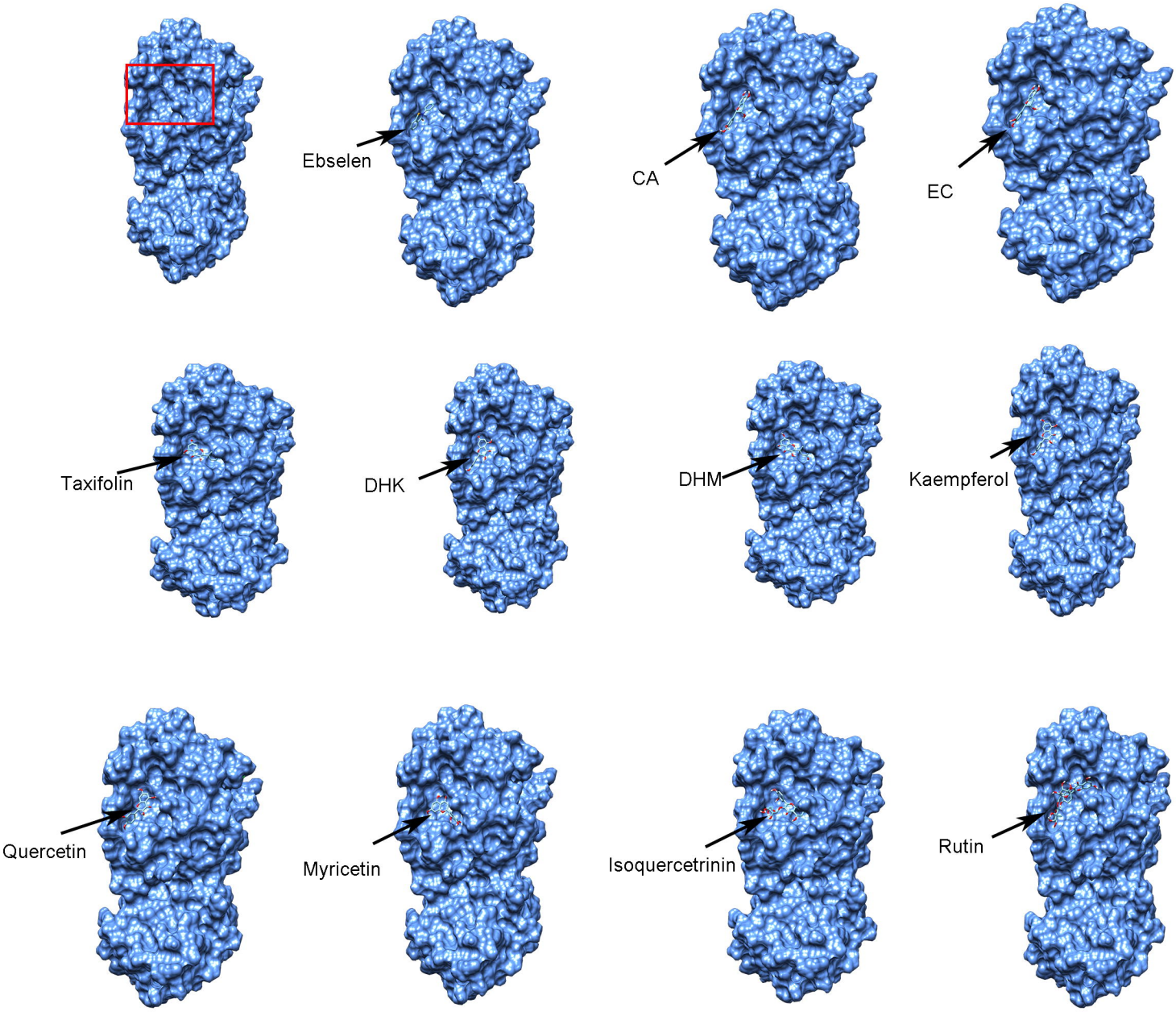
Ebselen
CA
EC
Taxifolin
DHK
DHM
Kaempferol
Quercetin
Myricetin
Isoquercetrinin
Rutin

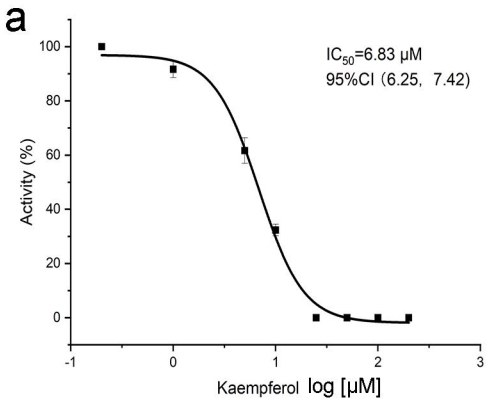
a
IC50=6.83 μM
95%CI (6.25, 7.42)
Activity (%)
Kaempferol log [μM]

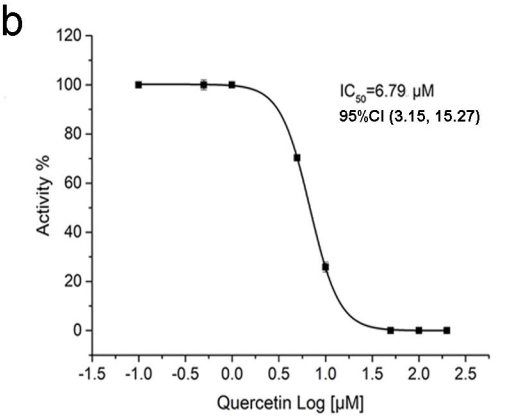
b
IC50=6.79 μM
95%CI (3.15, 15.27)
Activity %
Quercetin Log [μM]

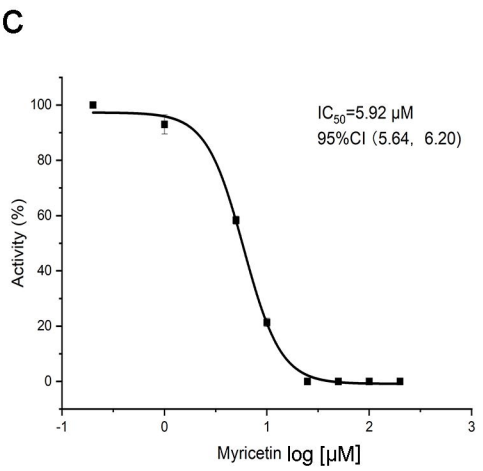
c
IC50=5.92 μM
95%CI (5.64, 6.20)
Activity (%)
Myricetin log [μM]

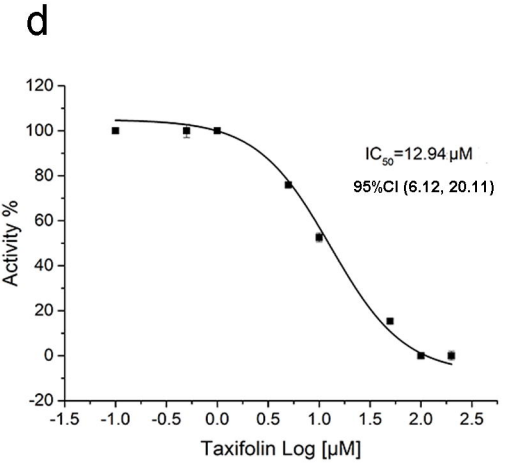
d
IC50=12.94 μM
95%CI (6.12, 20.11)
Activity %
Taxifolin Log [μM]

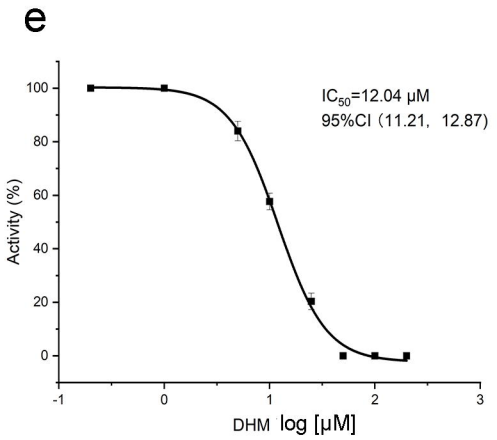
e
IC50=12.04 μM
95%CI (11.21, 12.87)
Activity (%)
DHM log [μM]

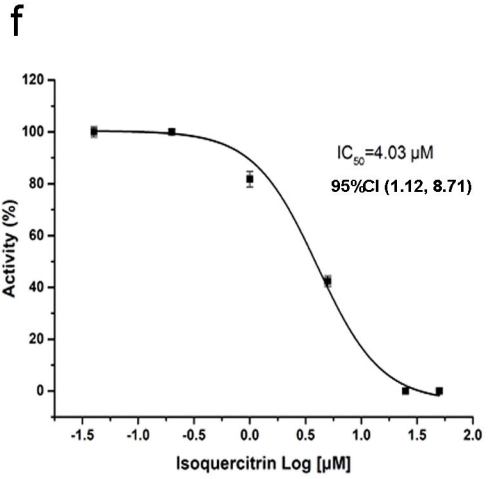
f
IC50=4.03 μM
95%CI (1.12, 8.71)
Activity (%)
Isoquercitrin Log [μM]

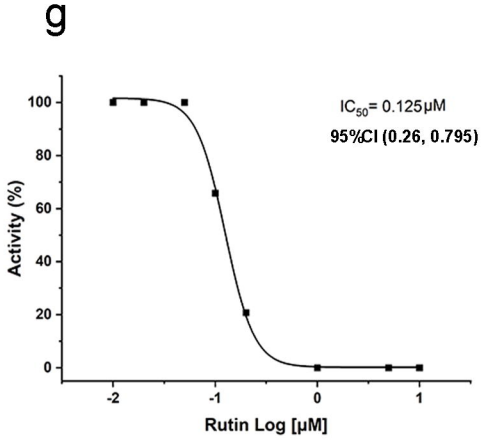
g
IC50= 0.125μM
95%CI (0.26, 0.795)
Activity (%)
Rutin Log [μM]

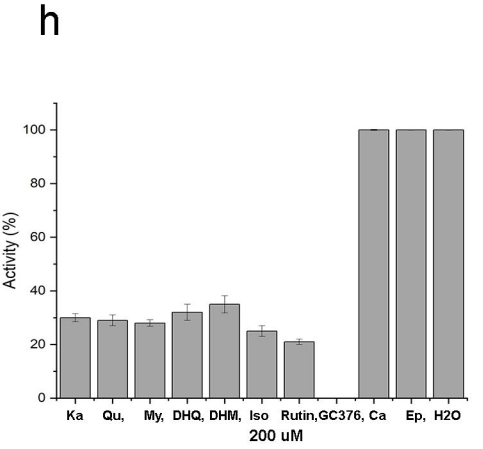
h
Activity (%)
Ka
Qu,
My,
DHQ,
DHM,
Iso
Rutin,
GC376,
Ca
Ep,
H2O
200 uM

a

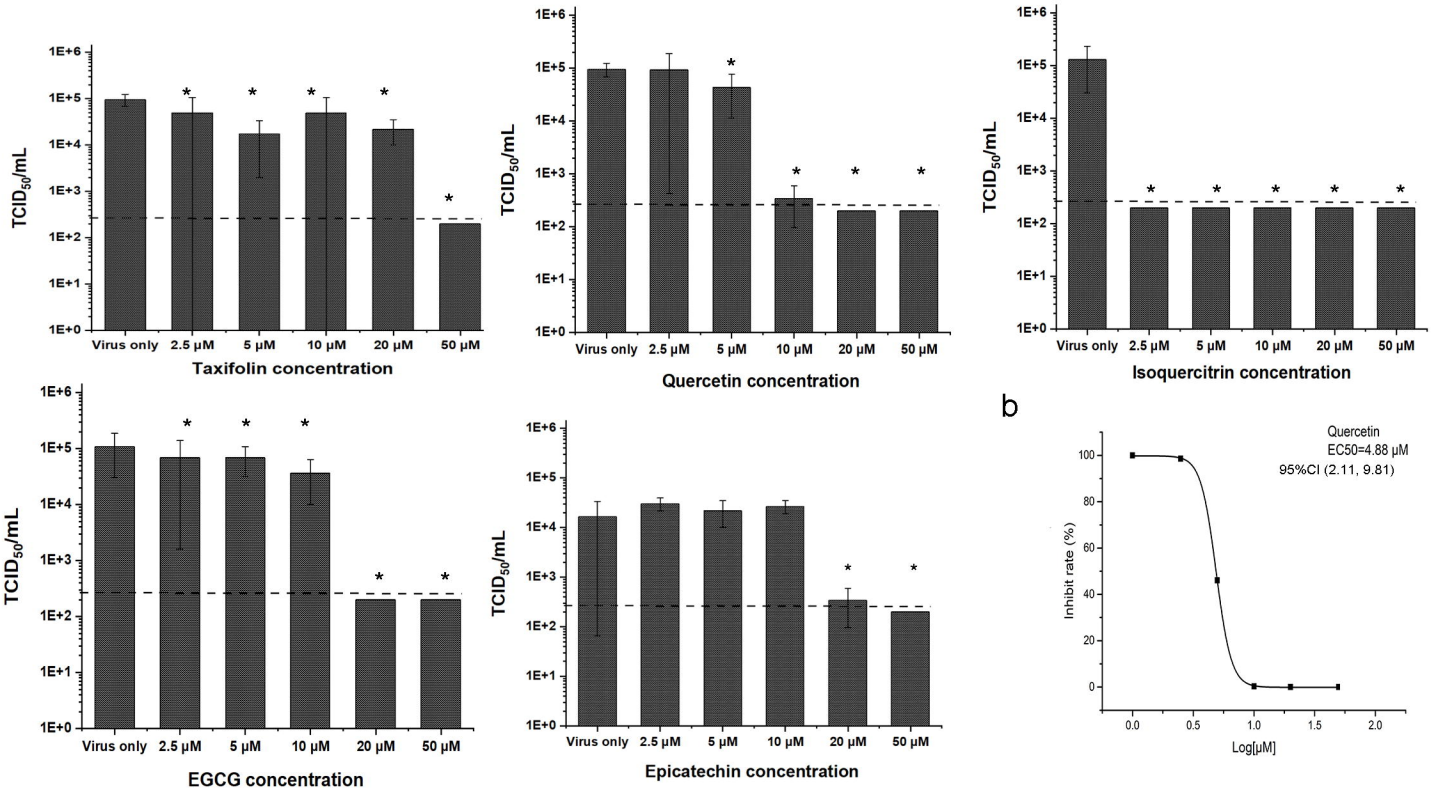
TCID50/mL
1E+6
1E+5
1E+4
1E+3
1E+2
1E+1
1E+0
Virus only
2.5 μM
5 μM
10 μM
20 μM
50 μM
Taxifolin concentration
Quercetin concentration
Isoquercitrin concentration
EGCG concentration
Epicatechin concentration
b
Quercetin
EC50=4.88 μM
95%CI (2.11, 9.81)
Inhibit rate (%)
100
80
60
40
20
0
0.0
0.5
1.0
1.5
2.0
Log[μM]